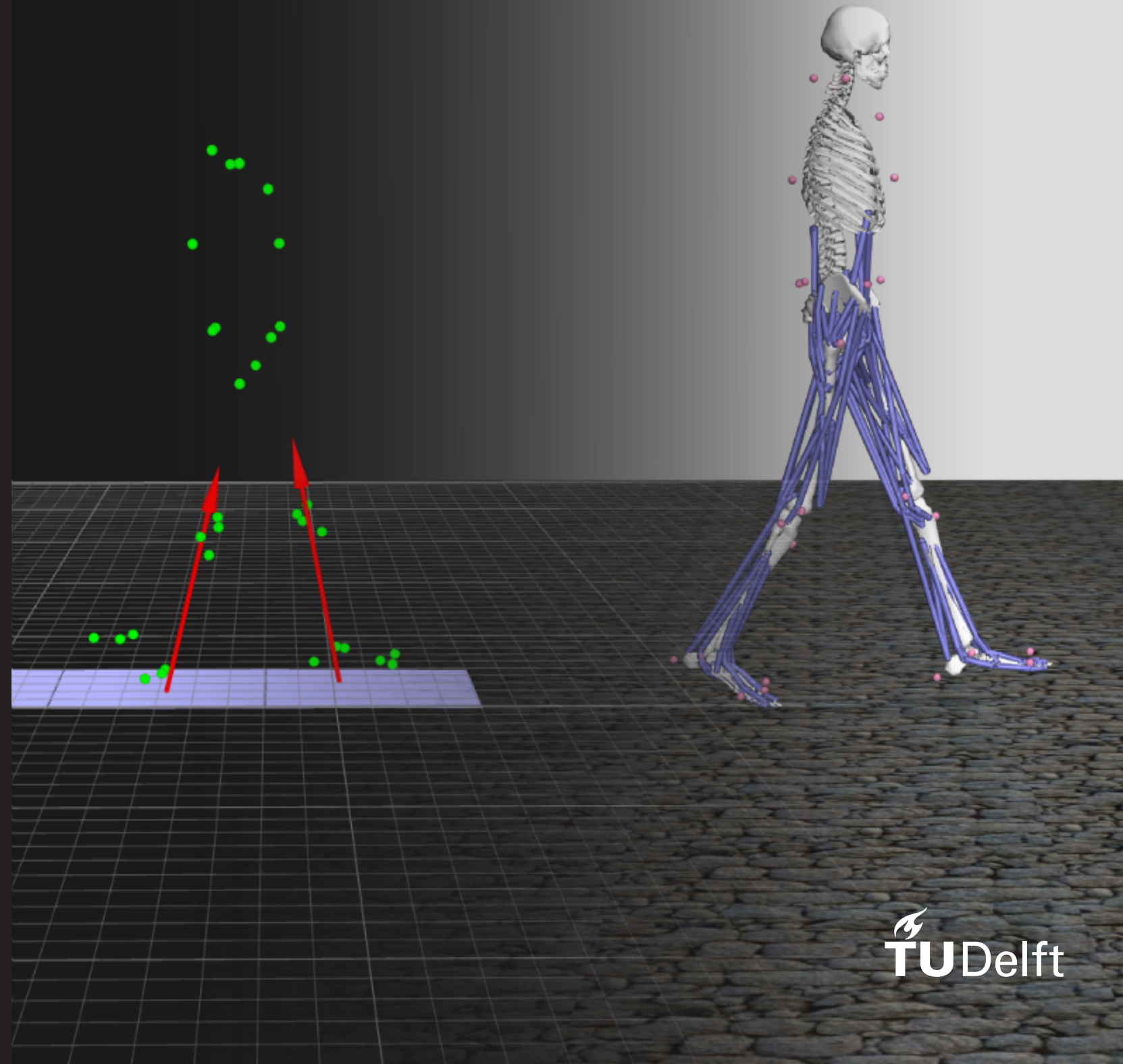


MSc Thesis

Multi-Metric Optimization for Human Walking

S. Kapteijn



Multi-Metric Optimization for Human Walking

MASTER OF SCIENCE THESIS

by

S. Kapteijn

to obtain the degree of Master of Science
at the Delft University of Technology,
to be defended publicly on May 19, 2022.

Student number:	4301242	
Thesis committee:	Dr. ir. L. Peternel,	TU Delft, supervisor,
	Dr. ing. L. Marchal Crespo,	TU Delft, committee chair and supervisor,
	Dr. ir. W. Kim,	Hanyang University, Seoul, supervisor,
	Dr. ir. A. Seth,	TU Delft, external member.

An electronic version of this thesis is available at <https://repository.tudelft.nl/>.

PREFACE

This thesis is the final part of my master Mechanical Engineering, track Biomechanical Design, at the Delft University of Technology. It has been a long, educational journey and I am glad and proud to finish it.

In this thesis I have analyzed the human gait and created a novel method for gait optimization using multiple metrics. As part of the project, I performed several experiments. I would like to thank Judith Cueto Fernandez for helping me out with the optical motion capture experiments and Micah Prendergast for assisting me with the joint fatigue calibration experiments. Furthermore, I would like to thank my supervisors, Luka Peternel, Laura Marchal Crespo, and Wansoo Kim, not only for their guidance during the project but also for supporting me in the more difficult moments that are also part of doing your master thesis. Finally, I would like to thank my family and friends for always supporting me throughout the process.

Stephan Kapteijn
Delft, May 2022

CONTENTS

I	Introduction	1
II	Methods	3
II-A	The framework	3
II-B	Motion data acquisition	4
II-B1	Hardware / Equipment	4
II-B2	Gait variations	4
II-C	Inverse Kinematics & Inverse Dynamics	5
II-D	Joint fatigue modeling	5
II-E	Manipulability analysis	6
II-E1	Manipulability calculation	6
II-E2	Manipulability analysis of the gait	6
II-F	Multi-metric optimization	7
II-F1	Optimization problem formulation	7
II-F2	Metrics	7
II-F3	Data normalization	8
II-F4	Brute-force optimization	8
III	Results	8
III-A	Visualisation of recorded gaits	9
III-B	Joint angle and joint torque verification	9
III-C	Effect of gait parameters on metrics	9
III-C1	Joint torque	9
III-C2	Joint fatigue	9
III-C3	Manipulability	12
III-D	Multi-metric optimization	12
IV	Discussion	13
V	Conclusion	13
	References	14
	Appendix	16
A	Motion Capture Experiment: Optical marker locations	16
B	Gait parameters recorded gaits	17
C	Joint fatigue parameter estimation	18
D	Manipulability analysis results	19
E	Elaborate cost table	21
F	Elaborate discussion: Effect of gait parameters on metrics	22
F1	Joint torque	22
F2	Joint fatigue	22
F3	Manipulability	22

Multi-Metric Optimization for Human Walking

Stephan Kapteijn¹

Supervised by: Wansoo Kim², Laura Marchal-Crespo¹, and Luka Peternel¹

Abstract—Walking is an essential part of almost all activities of daily living. Depending on the situation, different gait patterns can be observed, e.g., moving around the house, performing different sports, or even in case of injury. Even though the gait has been analyzed thoroughly for many decades, there are still some unexplored aspects that require more insight, especially those related to the influence of various parameters on the optimality and diversity of gait patterns. Many gait trajectory optimization strategies have been proposed in literature, however, most of them focus merely on optimizing for one metric (e.g., energy efficiency or joint torque). In this study, a multi-metric gait optimization framework is proposed, simultaneously accounting for joint torque, fatigue, and manipulability. To that end, 45 gaits, varying in stride length, step height, and walking speed, were recorded in a motion capture experiment, together forming a solution space of dynamically stable and physiologically feasible gaits, for the proposed optimization framework. Specific user needs (gait requirements) can be accounted for by adjusting the optimization weights, after which brute-force optimization is applied to either analyze the gait within the collected subspace or select the optimal gait with respect to desired parameters. Results are presented for a baseline case (with all optimization weights set to one), which can be used as a tool for gait analysis, in particular giving insights into specific aspects of the gait, e.g., joint loading, long-term performance, and capacity to sustain ground reaction forces (GRFs).

Keywords: gait optimization, multi-metric, joint fatigue, manipulability analysis

I. INTRODUCTION

Walking has been the primary form of human locomotion since immemorial time [1] and one of the primary forms of human transportation altogether as the versatility and ease of bipedal walking are hard to beat. Moreover, walking is an essential part of almost all activities of daily living [2] and each of these activities has a different goal. Due to our exceptional motor learning capabilities, humans are able to customize the gait, making it suitable for different purposes. For example, walking silently, or walking with reduced labor for the knee if it is injured. However, how humans perform this tailoring of the gait remains a partially unknown process.

What could help uncover this process is building an understanding of why a certain gait is effective in a specific situation, which could be done by gait analysis. Compared to where it started, gait analysis as it is known today has undergone a significant evolution [3]. It has transformed from a purely academic discipline to a useful tool in the hands of physicians and therapists [4]. It has become widely used as a means to understand particular deficits exhibited by a

patient, customize treatment, and monitor the effectiveness of this treatment [5]. For example, it has had a major impact on the way cerebral palsy is treated nowadays [6].

Typical elements of gait analysis are videotape examination, measurement of general gait parameters, kinematic analysis, kinetic analysis and electromyography (EMG) [4].

Kinematic analysis in its early stages consisted of manual digitization of film images and intensive kinematic computations to measure the limb positions [7]. Nowadays, we have motion capture technology to our aid. The gold standard in motion capture is optical motion capture, being able to achieve an accuracy of less than a millimeter for small volume captures [8]. Within optical motion capture, a distinction is made between passive marker-based, active marker-based, and markerless systems [9]. A passive system uses markers acting as reflectors, whereas the markers of an active system act as a light source. Markerless systems have the advantage that no markers have to be placed on the subject, however, the accuracy of these systems is not yet at the level of marker-based systems and it is still a hot research topic at the moment.

While motion capture can track the body segments' movements, force plates can measure the interaction of the body with the ground, or in other words the ground reaction forces (GRFs). These devices are essential in kinetic analysis. Being able to quantify kinetic parameters during walking, such as joint moments and joint power, is important, as these parameters are typically aimed to be modified with treatment of gait deficits [7].

Another technique applied in gait analysis is the measurement of gait parameters. Roberts et al. [10] have carried out extensive research into which biomechanical parameters are most relevant to evaluate during gait analysis of the healthy adult population. They found that spatio-temporal parameters such as walking speed, cadence, and step/stride length are the most often measured ones and they therefore claim that these parameters appear to be the most relevant ones in healthy adult gait analysis. However, this could be disputed, as the relevance depends gravely on the direction of the research. An advantage of these spatio-temporal parameters is that they are relatively easy to determine, compared to earlier mentioned kinetic parameters like joint moments and joint power, for which more computational procedures are required.

Finally, EMG can be applied in gait analysis to measure muscle activity during walking. The two main parameters that can be gained from EMG data are the timing and the relative increases/decreases of muscle activity during movements [11]. However, even though intense efforts have been done to find reliable methods to process and correctly interpret the muscle activation patterns during walking, the actual application in clinical practice is still limited [12].

¹Department of Cognitive Robotics, Delft University of Technology, Delft, The Netherlands.

²Department of Robotics, Hanyang University, Seoul, Korea.

Besides the analysis of already existing gaits, there is also much interest in the way gaits could be generated [13], [14]. This so-called gait trajectory generation has an important application in assistive devices (like exoskeletons for example), for which there is an increasing interest in the last years, reflected by the great number of reviews published about this subject recently [15]–[19]. There are assistive devices for healthy individuals, often focusing on power augmentation [20]–[24], as well as for individuals suffering from an impairment of some kind [25]–[29]. Furthermore, humanoid robotics is another major application of gait analysis and gait trajectory generation, since humanoid robots try to emulate human structure and behavior [30], [31].

To ensure that a certain gait is optimal for the activity that you plan to perform, some kind of gait optimization is required. For example, if it is desired to walk a large distance, you might want to optimize for a minimum energy consumption of the system. Alternatively, if you are recovering from an injury to the leg of some kind, you might want to minimize the loads to be endured by that leg during walking, or ensure not to exceed a certain joint torque.

For each optimization process, a careful selection of metrics is required. To modulate the amount of load being exerted on the body during walking, joint torque can be considered as metric for optimization. It is important to monitor the temporal load in order to prevent musculoskeletal injuries in humans or prevent exceeding the maximum power capacity of the robot's actuators. In Zhang et al. [32], optimization of the assistive torque applied by an ankle exoskeleton was performed, to minimize the metabolic energy cost of the subject. Furthermore, Channon et al. [33] performed gait optimization for a bipedal robot by minimizing the joint torques experienced during the single support phase and impact phase of the gait cycle.

Another approach to optimize for a minimum load to be sustained by the body is by analyzing the velocity and force manipulability. The manipulability of a mechanical system (e.g., human or robot) measures its capacity to transfer joint movements/torques into end-effector movements/forces as a function of the joint configuration [34]. It gives an indication of how well an end-effector of the mechanical system can produce force or velocity in certain directions of Cartesian space. Considering this metric could therefore help determine the leg configuration that is optimal for sustaining external forces, like GRFs, during the gait. An advantage of the manipulability over joint torque is that it can also be applied to determine the optimal leg configuration in terms of good velocity production. However, joint torque estimation is still important on its own to account for overloading joint torques, thus these metrics complement each other.

Recent studies on manipulability analysis of human walking show that the kinematic manipulability of the swing foot can characterize the selection of strategies at different stages of the swing phase [35], [36]. Similarly, Fard and Mosadeghzad [37] proposed utilizing the manipulability in selecting an appropriate postural strategy to restore stability when a perturbation during human walking occurs. Gait trajectory optimization was performed considering 1. only joint torque and 2. both joint torque and manipulability as metrics in the cost function and

the results indicate that including the manipulability improves the capability of rejecting the induced disturbances. Another example where the leg manipulability is utilized as metric is in the study done by Kim et al. [38], where gait pattern generation is performed for a powered robotic exoskeleton for assisting healthy humans, to improve the energy efficiency of the integrated system (meaning the human and exoskeleton together).

When long-term performance of the gait is desired, minimization of fatigue could be performed. Fatigue can be seen as the decline over time of the ability to generate force. Monitoring the fatigue could therefore assure that an individual can maintain a certain gait for a longer period of time. Fatigue minimization can be accounted for indirectly, by optimizing for low energy efficiency as done in [39], [40]. However, these studies do not provide a direct estimation of fatigue. A more direct way to optimize for fatigue is by using fatigue models. As fatigue is an integrated effort over time, the fatigue models available in literature can be distinguished by how they estimate the effort, e.g. by muscle activity [41] or by joint torque [42]–[44]. As we can see from the just mentioned selection of studies, fatigue modeling has been more commonly applied in studies for arms or the whole body during analysis and control of ergonomics in manufacturing processes. However, an example where fatigue is used as metric in gait optimization is Peasgood et al. [45], where the fatigue rate is minimized to optimize for the metabolic energy cost.

While the above-mentioned metrics all optimize for numerical objectives, one could also choose a different approach, taking the user preference into account for determining the optimal gait. In their study, Tucker et al. [46] proposed a personalized gait optimization framework, using the user preference (in terms of comfort) to determine the optimal gait. Ingraham et al. [47] investigated the users' repeatability in identifying their preferred assistance for bilateral ankle exoskeletons during walking and concluded that individuals are able to reliably identify their preferences.

Thus, gait optimization has been performed using different metrics in numerous studies, however, many focus merely on one metric. Only a few have done gait optimization that combined multiple metrics. Furthermore, while applying fatigue modeling in the field of ergonomics has already been investigated [41], [44], applying it in gait trajectory optimization is still quite unexplored.

To address the gap in literature, we created a modular framework for gait optimization for human walking, applicable for different contexts and goals, which combines multiple metrics: joint torque, fatigue, and manipulability. The joint torque was selected as metric to allow modulation of the loads exerted on the joints, which is relevant to prevent overloading of the musculoskeletal system. We selected manipulability because it gives an indication of how well the legs can produce or sustain motion and forces during different phases of the gait. Finally, to also account for the long-term performance of the gait, fatigue was selected. Due to the modularity of the framework, it can be easily adjusted as well as expanded enabling further development.

II. METHODS

A. The framework

An overview of the framework that was established in this thesis can be seen in Figure 1. It is a versatile framework, combining experimental procedures, computational procedures, and a multi-metric optimization method. Motion data is gathered during an optical motion capture experiment, kinematic and kinetic analysis are performed in OpenSim, manipulability analysis and joint fatigue modeling are done in MATLAB, and finally multi-metric optimization is performed producing an optimal gait for the specified optimization goal.

In this study, we considered three metrics: joint torque, fatigue, and manipulability, which will be examined in detail in the following subsections. We selected joint torque because it is important to prevent overloading of the musculoskeletal system. Fatigue was selected because it affects the long-term performance of the gait. Finally, we selected manipulability because it gives an indication of how well the legs can produce or sustain motion and forces during different phases of the gait. By selecting these metrics, some of the major aspects of the gait are covered. However, the framework is general in the sense that if needed, other metrics can be added to it. Furthermore, we made the framework modular, such that future studies in this area of research can easily utilize the framework for their own purposes, adding or replacing elements of the framework as desired.

The framework we built aims to aid in finding a gait that matches the needs of a specific user and use case. These needs can be driven by health requirements, for example when a particular gait is wanted for a patient recovering from a knee injury. Alternatively, these needs can be driven by performance, for example when a gait is desired that can be sustained for as long as possible. The requirements formed in this way are what determine the optimization goal. Since there is a wide variety of optimization goals that can be specified, a broad data set is desired, containing some degree of variation. Rather than studying the natural gait of several different subjects, we decided to study a broad set of gait variations created by one subject. Furthermore, gait optimization is typically subject-specific. To obtain the required degree of variation for a specific subject, the motion data was collected by performing an optical motion capture experiment. The reason for choosing to work with experimentally collected data rather than simulated data is that experimentally collected data is already subject-specific and conforms with physiological feasibility and dynamic stability constraints. This approach is also common in literature [48]. As the human gait is an extremely complex movement with many possible solutions, it is difficult to create an optimization that delivers only feasible gaits in an efficient manner. This is because the search space for the optimization to be performed is incredibly large, taking into account that each combination of joint angles and walking speeds results in a different gait. Many of those gaits might for example be physiologically unrealistic, or they might be dynamically unstable. To ensure that the output of the framework will contain solely feasible gaits, we decided to

create our own search space filled with gaits recorded during an optical motion capture experiment (see Section II-B).

An extra benefit of incorporating the motion recording experiment in the framework is that it gravely reduces the required computational resources, as the search space is reduced to only a small set of feasible gaits. In turn, it enlarges the set of viable optimization methods that can be efficiently applied to solve the problem. For example, this makes it possible to employ even brute-force optimization which is guaranteed to find a global maximum within this limited space of recorded solutions. Often, this optimization method is not considered as it is too computationally intensive, however, in our case, it becomes a viable option and was thus employed to find specific gaits. Section II-F discusses some possible optimization methods and further elaborates on the choice for brute-force optimization.

In order to really take a next step in generating gaits for various purposes, we tried to combine the knowledge that is already available from previous works and then expand it. MATLAB and OpenSim were the main computational tools used for this. As OpenSim is an established tool for modeling musculoskeletal processes [49], it was used to perform modeling and simulation of the walking motion. Inverse kinematics (IK) was performed using the marker data, acquired by the optical motion capture experiment, to determine the exact body configurations during the gait cycle. Then inverse dynamics (ID) was performed, using the external loads (i.e. the GRFs) to find the net forces and torques at each joint responsible for the movement.

OpenSim modeling is based on solving the dynamics of the human body. The following equations of motion describe the simplified internal dynamics model:

$$\tau_{dyn} = M(q)\ddot{q} + C(q, \dot{q})\dot{q} + G(q), \quad (1)$$

where M is the system mass matrix, C is the vector of Coriolis and centrifugal forces, G is the vector of gravitational forces, and q and its derivatives are the generalized joint positions, velocities, and accelerations. Since the human body is also interacting with the ground, we then also need to account for external forces F_{ext} , where the net joint torques are determined by

$$\tau = J^T(q)F_{ext} + \tau_{dyn}(q, \dot{q}, \ddot{q}). \quad (2)$$

where J is the Jacobian matrix, responsible for transforming the external loads F_{ext} to the body. These external loads are the GRFs that are measured by force plates during the motion capture experiment. Section II-C will elaborate further on the IK and ID processes.

The joint torque computed in Equation 2 will be used as one of the metrics in the optimization process (see Section II-F2). Furthermore, the joint torque is also used as input for the joint fatigue model, as can be seen in Figure 1. Fatigue can be seen as effort integrated over time and the model that is used in this framework uses the joint torque as an estimation of the effort. Section II-D will elaborate on the joint fatigue computation and will go into how the joint fatigue parameters, required for the model, were determined.

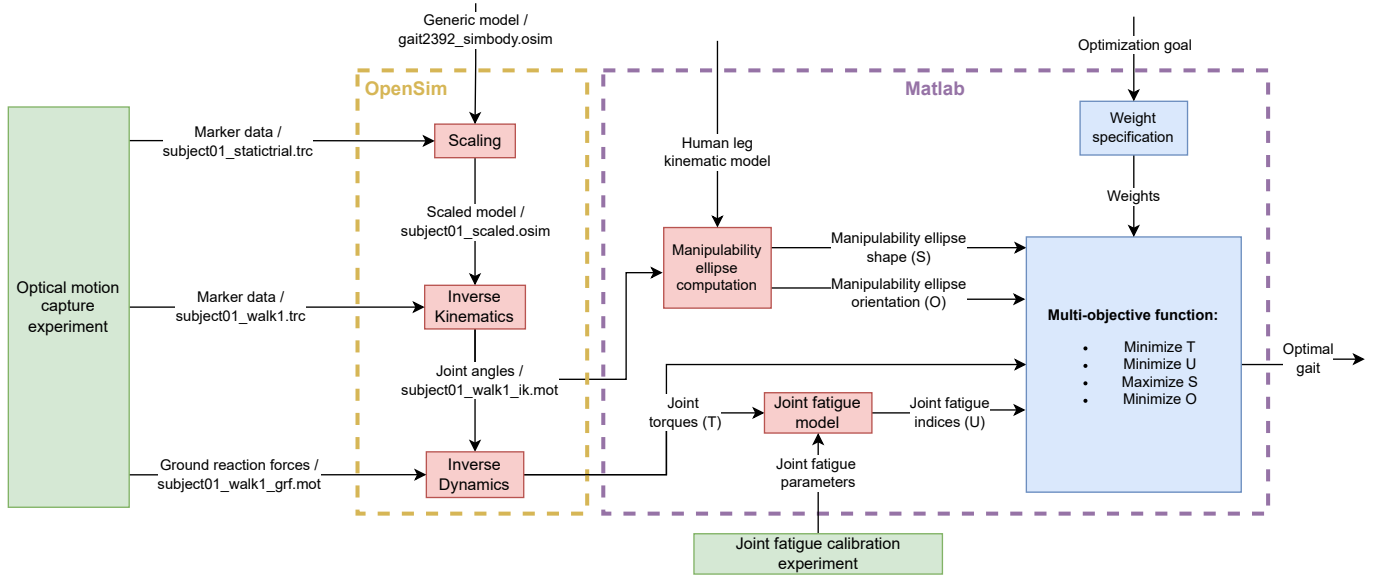


Fig. 1. Overview of the established framework, containing experiments (green), modeling/computational methods (red) and an optimization step (blue). The main tools used for computation are OpenSim (dashed yellow box) and MATLAB (dashed purple box).

The Jacobian matrix J from Equation 2, which is used to map the GRFs to the body, is also an important factor in the manipulability analysis. As manipulability has not often been applied in gait analysis yet, we hope to cover some new ground by incorporating it into our framework. Section II-E explains how the concept of manipulability is used to analyze the recorded walking motions and why we decided upon using the manipulability ellipse shape and orientation as metrics for the optimization process.

While the dynamic model equations 1 and 2 describe a general 3D case, we limited this study to the sagittal plane. This simplification can be made without too many consequences as, according to Eng and Winter [50], 74% of the total work done at the hip was being done in the sagittal plane. Similarly, for the knee and ankle, 85% and 93% of the work was done in the sagittal plane, respectively.

B. Motion data acquisition

1) *Hardware / Equipment:* The gait recordings were performed in the BioMechaMotion Lab of the department of BioMechanical Engineering at the TU Delft. Marker-based motion capture was performed, using the marker-tracking system from Qualisys (Sweden), which included 12 Oqus 700 infrared cameras for tracking the optical markers and two Oqus 210c cameras for recording video footage. The GRFs were measured using five force plates of KISTLER (Switzerland), three of type 9260AA6 and two of type 9260AA6, which were laid down consecutively, creating a path of force plates. These data streams are acquired and synchronized by the software application QTM (Qualisys Track Manager). In figure 2 the setup of the experiment can be seen and in Appendix A we elaborate on the locations of the optical markers.

2) *Gait variations:* The data set contains gaits varying in: 1. stride length, 2. step height, and 3. walking speed. It was decided that each of these parameters can either have a

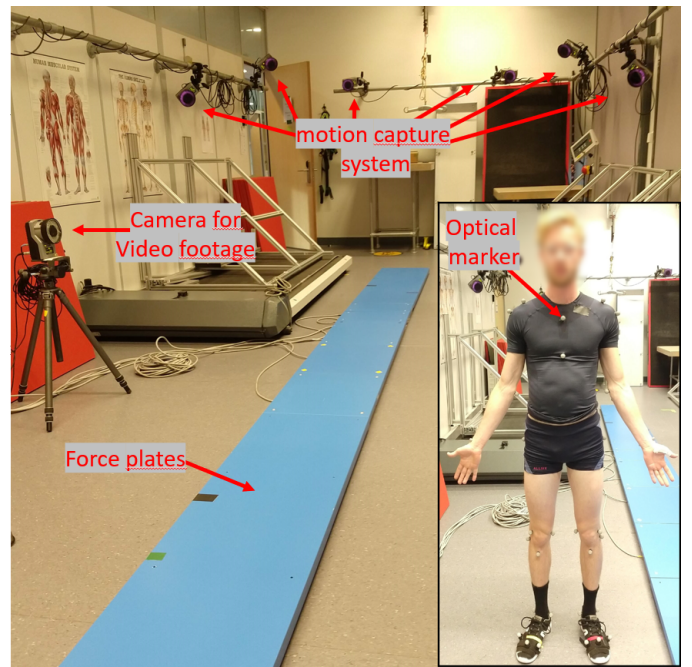


Fig. 2. Experiment setup including five force plates, 12 infrared cameras and two cameras for video footage. 44 optical markers were placed on the subject's body.

low, medium or high value and a gait was recorded for each possible combination of these parameters, resulting in 27 gaits. This set of gaits will be referred to as the basic data set from now on.

The naming convention used for the recorded gaits in the remainder of this thesis is based on these parameters. For example, a gait with a low stride length, high step height, and a medium walking speed is called LowHighMid. It should be emphasized that only one of the recorded gaits is a natural

gait, whereas the other gaits are consciously performed. The natural gait, indicated by the name MidLowMid, served as the basis for the data set in the sense that the other recorded gaits were variations with respect to this natural gait.

Additionally, some extra variations of walking were performed, with bent knees, leaning forward, and leaning backward. By adding these out-of-the-box recordings to the data set, we enabled the framework to possibly produce an unexpected outcome. This part of the data set contains 18 gaits and will be referred to as the additional data set from now on. A list of the total data set, comprising 45 gaits, can be seen in Appendix B. There, the stride length, step height, walking speed, and cadence are also given for each gait.

C. Inverse Kinematics & Inverse Dynamics

The freely available OpenSim software [49] was used as a tool for modeling and simulating the gaits that were acquired with motion capture. The generic gait 2392 OpenSim model was utilized for this. It is a 23-degree-of-freedom lower extremity musculoskeletal model, containing 92 musculotendon actuators, created mainly for gait analysis. The model was first scaled to the proportions of the subject's body, using a marker set created to be identical to the marker set used during the motion capture experiment, seen in figure 9 in Appendix A.

The marker data collected during the motion capture experiment contain the 3D locations of each marker. To translate these marker locations to orientations of the leg segments and thus to the joint angles, inverse kinematics (IK) was applied. As can be seen in Figure 1, the OpenSim IK tool requires the scaled musculoskeletal model and the marker locations, and determines the joint angles throughout the gait cycle.

Then, inverse dynamics (ID) was applied, using Equations 1 and 2, to find the net torques at each joint responsible for the motion determined by IK. The OpenSim ID tool requires the GRFs, measured by the force plates, and the joint angle data following from IK as inputs and produces the joint torques as output. Since we are analyzing the gaits solely in the sagittal plane, mainly the hip flexion/extension, knee flexion/extension, and ankle plantar flexion/dorsiflexion angles and torques were used in further analysis.

By analyzing several gait cycles of one gait recording and comparing the joint angle/torque trajectories between these gait cycles, a measure of the repeatability of the trajectories could be obtained. This provides an indication of the reliability of the IK and ID processes. Due to time constraints, it was decided to perform this verification process for only a portion of the total data set: MidLowMid, LowLowHigh, BentLowHighMid, LeaningForwardMidHighMid, and High-HighLow. With this selection, it was attempted to represent the total data set as well as possible by selecting gaits that all differ from each other considerably. For each of these gait recordings, the heel strikes were determined manually by analyzing when the force plate that was being stepped on would give a nonzero value. Two gait cycles were isolated for comparison, by selecting the data between heel strikes, and the data were resampled to 300 data points to ensure the data sets were of equal length.

To account for small timing mismatches between the two gait cycles, dynamic time warping (DTW) was performed using the MATLAB built-in dtw function. This method stretches the two input vectors such that the sum of the euclidean distances between the data points is the lowest, and this sum of Euclidean distances is also its output. A more detailed explanation of the DTW process is given in [51]. The mean absolute error (MAE) was then computed by dividing the sum of Euclidean distances by the number of data points (300). To get a more intuitive sense of how large this error is with respect to the data that was analyzed, the percentage error (PE) was then computed by normalizing the MAE with respect to the range of the trajectories, with the range being the maximum angle/torque value minus the minimum angle/torque value of the trajectory during one gait cycle.

In Section III, joint angle trajectories for multiple recorded gaits are shown, in combination with visualizations of these gaits, and the percentage errors of the verification process are given.

D. Joint fatigue modeling

Several models can be found in literature for estimating fatigue [52]–[55], mostly relying on complex biomechanical systems. While applying such a model might provide a very precise fatigue estimation, it also brings some complexity to the analysis. In essence, fatigue is an integrated effort over time. Thus, by acquiring an estimation of effort, we could model fatigue in a more simple manner than in some of the above-mentioned studies. Some studies that have performed fatigue modeling through effort estimation are [42]–[44], which use joint torque as indication of effort. For the fatigue estimations performed in this thesis, we used the model from [44], which is described by

$$\frac{du_i(t)}{dt} = \begin{cases} (1 - u_i(t)) \frac{|\tau_i(\mathbf{q}, t)|}{\lambda_i} & \text{if } |\tau_i(t)| \geq \tau_{th,i} \\ -u_i(t) \frac{R}{\lambda_i} & \text{if } |\tau_i(t)| < \tau_{th,i} \end{cases}, \quad (3)$$

where u_i is the fatigue index for the i -th joint, τ_i is the joint torque for the given time t , λ_i is the parameter that determines the joint-specific fatigue characteristics, R is the recovery rate, specifying how fast the joint recovers when it is resting and $\tau_{th,i}$ is the torque threshold that determines if the fatigue of the joint is increasing or decreasing. The model is inspired by RC circuit dynamics and has a shape similar to that of an exponential charge/discharge function. It was decided to rewrite Equation 3 into recursive form as

$$u_{i,t+1} = \begin{cases} u_{i,t} + (1 - u_{i,t}) \frac{|\tau_{i,t}|}{\lambda_i} \Delta t & \text{if } |\tau_{i,t}| \geq \tau_{th,i} \\ u_{i,t} - u_{i,t} \frac{R}{\lambda_i} \Delta t & \text{if } |\tau_{i,t}| < \tau_{th,i} \end{cases}. \quad (4)$$

The recovery rate R was set to a conservative value of 0.5, as was also done in [44] and [41]. Parameter λ was determined by several calibration experiments, similar to the experiment proposed in [41]. Two measurements were performed for each joint, one for flexion and one for extension direction in the sagittal plane, thus 12 measurements in total. During each of these measurements, the subject was instructed to produce maximum torque and try to maintain this torque level for as

long as possible. The time T_{ref} was measured up to the point that the subject could not endure this torque level anymore. Note that this procedure is subject-dependant, as the subject was instructed to stop when maintaining the torque level would become uncomfortable. Since the model follows an exponential charge function that mathematically never reaches the maximum value of 1, i.e. 100%, we needed to select some value considered as maximum. In electronics, where exponential charge functions are common, it is typical to assume that a capacitor is fully charged after five time constants. Similarly, the maximum value of the joint fatigue parameter u was assumed to be reached after five time constants, thus when $u = 0.993$. Fatigue capacity parameter λ could then be derived for each joint (in both flexion and extension direction) by

$$\lambda = -\frac{|\tau_{ref}| \cdot T_{ref}}{\ln(1 - 0.993)}, \quad (5)$$

where T_{ref} is the time that the reference torque τ_{ref} could be maintained by the subject.

The estimated λ parameters slightly differed for the left and the right leg. Bilateral symmetry was assumed, thus the λ value of the weakest leg was selected and the corresponding joint of the other leg was assigned with the same value. The weakest leg was selected to stay on the conservative side with our assumption. This resulted in the set of λ parameters seen in Table I. Further details of the calibration experiments are provided in Appendix C, together with visuals of the experiment setup.

TABLE I
JOINT SPECIFIC FATIGUE PARAMETERS λ AND τ_{th} .

	Hip flexion	Knee flexion	Ankle dorsi-flexion	Hip extension	Knee extension	Ankle plantar-flexion
λ (Nms)	444	282	75.8	754	550	2.15e+3
τ_{th} (Nm)	0.177	0.133	0.046	-0.234	-0.184	-0.295

Finally, the torque thresholds τ_{th} , determining whether the joints are increasing or decreasing their fatigue levels, had to be determined. During each of the fatigue calibration experiments, the subject was instructed to produce maximum torque with that specific joint. Therefore, these reference torques can be interpreted as an indication of the general strength of the joints with respect to each other. Consequently, the torque thresholds were scaled to one another according to the ratio between these reference torques. Therefore, only one torque threshold had to be selected and the other thresholds could be computed through this interdependency. For each joint, the torque threshold of the weakest leg was selected and the corresponding joint of the other leg was assigned with the same value, similar to the computation of the λ parameters. Table VIII in Appendix C gives an overview of all the reference torques τ_{ref} , fatigue parameters λ and torque thresholds τ_{th} that were determined in the calibration experiments.

To find a somewhat realistic set of torque thresholds, an assumption was required for a reasonable fatigue index after a certain time. Since no literature specifically defines a realistic

fatigue index after a certain time, we made the following assumption: after half an hour of regular walking, an average fatigue index of 20% is expected. This assumption will be further discussed in Section IV. An initial guess was made for the set of torque thresholds and the average fatigue index was calculated. Then, depending on this value, the set of torque thresholds was adjusted. This process was iterated until the average fatigue level of 20% was achieved, resulting in the set of thresholds seen in Table I.

E. Manipulability analysis

In robotics, manipulability is a measure of how well the end-effector can produce force and/or motion in all directions and is often used to visualize how close a robot is to being in a singular configuration [34]. In the case of a 3D environment, it can be visualized as an ellipsoid, and for a 2D environment as an ellipse. The length of the vector from the center of the ellipsoid/ellipse to the surface indicates how well the limb can produce motion/forces in that specific direction of Cartesian space.

1) *Manipulability calculation:* Multiple manipulability measures have been defined in previous works. The classical one is the scalar manipulability, defined by Yoshikawa [34] as

$$w = \sqrt{\det(\mathbf{J}(\mathbf{q})\mathbf{J}(\mathbf{q})^T)}, \quad (6)$$

where J is the Jacobian matrix at joint configuration q . The scalar manipulability is proportional to the volume of the manipulability ellipsoid [56] and is especially interesting in a case where both motion and force are to be optimized together.

However, in this research, we are applying manipulability analysis on walking, in which several phases can be identified where the capability to produce motion is more relevant, and several phases where the propulsion or absorption of force is more relevant. Using singular value decomposition, the manipulability can be analyzed on a more detailed level. Then, if it is desired to focus on the capability to produce motion, we can derive the velocity manipulability by

$$\mathbf{U}\Sigma\mathbf{V}^T = \mathbf{J}(\mathbf{q})\mathbf{J}(\mathbf{q})^T, \quad (7)$$

where U and V are matrices containing the left and right singular vectors respectively and Σ is a diagonal matrix containing the singular values. Since velocity and force manipulability are orthogonal, the force manipulability is obtained by the inverse of (7).

The orthogonality of the force and velocity manipulability can be seen in Figure 3, where both ellipses are schematically visualized during toe-off, with the toe as end-effector. The singular vectors present in matrix U represent the direction of the velocity/force ellipsoids axes (indicated by v in Figure 3), or in other words the **orientation** of the ellipsoid. The singular values indicate the magnitude of the axes (indicated by $\sqrt{\mu}$ in Figure 3) and therefore represent the **shape** of the ellipsoid.

2) *Manipulability analysis of the gait:* The gait cycle can be separated into two main phases: the stance and swing phase [57]. The stance phase is initiated by initial contact (IC) (also called heel strike), where the heel touches the ground. The leg touching the ground is then called the dominant leg in this

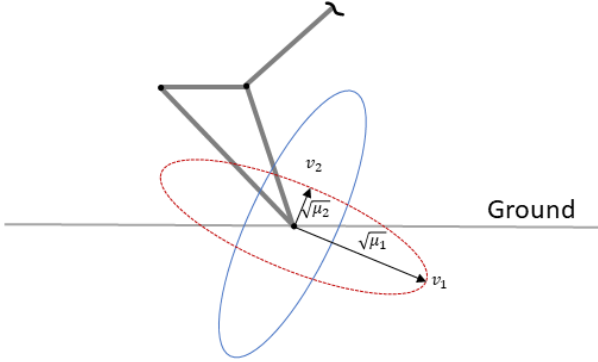


Fig. 3. Schematic drawing of foot with the velocity ellipse in red (dashed line) and force ellipse in blue (solid line) during toe-off. Note that v and μ are drawn only in the velocity ellipse, but can be drawn in the force ellipse in a similar fashion.

cycle. The stance phase can be further divided into loading response, mid-stance, terminal stance, and pre-swing. During loading response, the impact of the foot on the ground is absorbed and the bodyweight is transferred onto the dominant leg. The mid-stance and terminal stance phases together form the single-limb support phase, starting and ending when the non-dominant leg leaves the ground (opposite toe-off (OTO)) and touches the ground again (opposite initial contact (OIC)), respectively. During those phases, the body weight is carried solely by the dominant leg. The body is then propelled by the dominant leg during pre-swing. As each of these first four gait phases revolves around absorbing, carrying, or generating force, the focus of the manipulability analysis for these phases is on the force ellipse, as seen in Table II. The swing phase can be divided into initial swing, mid-swing, and terminal swing. During the swing phase, the limb is advanced, going through three phases, lifting itself (initial swing), advancing (mid-swing), and preparing for the next stance phase (terminal swing). As these phases focus on the advancement of the limb, the velocity ellipse is analyzed.

TABLE II
OVERVIEW OF THE SELECTED LEG ENDPOINT AND ELLIPSE TYPE ANALYZED FOR EACH GAIT PHASE DURING THE GAIT CYCLE.

	Gait phase	Leg endpoint	Ellipse type
Stance phase	Loading response	Heel	Force
	Mid-stance	Heel	Force
	Terminal stance	Toe	Force
	Pre-swing	Toe	Force
Swing phase	Initial swing	Toe	Velocity
	Mid-swing	Toe	Velocity
	Terminal swing	Toe	Velocity

During loading response the contact with the ground of the dominant leg is provided only by the heel, so the heel is chosen as endpoint for generating the force ellipse during that phase. For mid-stance, where the body weight is slowly transferred from the heel towards the toe of the dominant leg, the heel was chosen as endpoint as well. For all the other phases, the velocity and force ellipses were generated with the toe as endpoint.

F. Multi-metric optimization

1) *Optimization problem formulation:* The aim of optimization in this framework is to find an optimal gait for a certain optimization goal using joint torque, joint fatigue, and manipulability as main parameters in the optimization process. The optimization problem can be formulated by

$$H = \arg \min_{q, \dot{q}, \ddot{q}} \left(\sum_{i=1}^n (w_{t,i} \cdot T_i) + \sum_{i=1}^n (w_{u,i} \cdot U_i) - \sum_{j=1}^m (w_{s,j} \cdot S_j) + \sum_{j=1}^m (w_{o,j} \cdot O_j) \right), \quad (8)$$

where q , \dot{q} and \ddot{q} are the generalized joint positions, velocities and accelerations, T_i and U_i are metrics representing the joint torque and joint fatigue for the i -th joint, respectively, S_j and O_j are metrics representing the manipulability ellipse shape and manipulability ellipse orientation for gait phase j , respectively, and $w_{t,i}$, $w_{u,i}$, $w_{s,j}$ and $w_{o,j}$ are weights corresponding to these metrics. Finally, n is the number of joints taken into account in the optimization process, in our case six (hips, knees, and ankles), and m is the number of gait phases, in our case seven (see Table II).

To clarify, $\arg \min$ finds the argument to the function that results in the minimum output. Therefore, Equation 8 determines the motion (defined by q , \dot{q} and \ddot{q}), that results in the lowest total cost, where the total cost consists of terms associated with joint torque, joint fatigue, and manipulability.

The weights $w_{t,i}$, $w_{u,i}$, $w_{s,j}$ and $w_{o,j}$ can be used to specify a certain optimization goal. For example, increasing weights $w_{t,1}$ and $w_{t,2}$ will increase the importance of minimizing the joint torque metrics of the first and the second joint in the cost function. Or if one searches a gait where the occurrence of joint fatigue is not relevant, weights $w_{u,i}$ can be put to zero. However, as the emphasis of this research is on presenting this new framework rather than applying it to study cases, for now, a general weighting of 1 was applied to all the weights.

Note that the ellipse shape S has a minus sign in the cost function, while the other metrics T , U , and O have a plus sign. This is the case as maximizing S feels more intuitively correct, in contrast with the other metrics. However, in the case that S is to be minimized, or in the case that the other metrics T , U and O are to be maximized, their respective plus/minus sign can simply be changed by assigning negative values to their respective weights ($w_{s,j}$, $w_{t,i}$, $w_{u,i}$ and $w_{o,j}$).

2) *Metrics:* The joint torque metric T for a joint i is specified as

$$T_i = |\overline{\tau_i(t)}|, \quad (9)$$

where τ_i is the i -th joint torque trajectory throughout one gait cycle. So the mean value is computed over the absolute torque trajectory. In this way, we can get a general sense of the magnitude of the load exerted on the specific joint.

The joint fatigue metric U for a joint i is described by

$$F_i = u_{i,t_{end}} \quad (10)$$

with $u_{i,t_{end}}$ representing the i -th joint fatigue index following from Equation 4, at the last instant of the gait cycle. By picking

the fatigue index at this instant, we get an impression of how much fatigue has built up in the joint during one gait cycle, which indicates how exhausting the gait was for the specific joint i .

The manipulability ellipse shape S for gait phase j can be described by

$$S_j = \overline{r(t)}, \quad \text{with} \quad r(t) = \sqrt{\frac{\mu_1(t)}{\mu_2(t)}}, \quad (11)$$

where $\mu_1(t)$ and $\mu_2(t)$ are the singular values at time instant t following from Equation 7. Ellipse shape S is then determined by averaging the ratio $r(t)$ over the specific gait phase. The minimum value that S can reach is 1, which occurs when the ellipse axes are of equal magnitude, making the ellipse a circle. When the velocity/force ellipse is more flat, S will have a higher value and vice versa. A higher value of S will mean that, in the direction of the major axis, more velocity/force (depending on the ellipse type) can be produced.

Finally, the manipulability ellipse orientation O for gait phase j is represented by

$$O_j = |\overline{\theta(t)}|, \quad \text{with} \quad \theta(t) = \tan^{-1} \left(\frac{v_{1,y}(t)}{v_{1,x}(t)} \right) - \theta_{ref} \quad (12)$$

where $v_{1,x}(t)$ and $v_{1,y}(t)$ are the x and y components of singular vector v_1 at time instant t found from Equation 7, corresponding to the major axis of the velocity/force ellipse. θ_{ref} is a reference angle, defined to enable the designation of a baseline orientation that is desired for the ellipse. Finally, $\theta(t)$ is called the deviation angle and it is the angle between the major axis of the ellipse and the reference angle θ_{ref} . Ellipse orientation O is then computed by taking the mean value of the absolute deviation angle $\theta(t)$.

For gait phases where the velocity ellipse was selected for analysis, it was decided to choose θ_{ref} parallel to the ground. In this way, velocity in the forward direction, i.e. the walking direction, is rewarded positively in the cost function. For gait phases where the force ellipse is analyzed, θ_{ref} should ideally be aligned with the direction of the GRF, as is done in [38]. Then, during heel strike the interaction forces could be absorbed optimally and during toe-off, the foot could propel the body most efficiently. However, to simplify computational matters and since visual inspection of the recorded motion data showed that the GRF often points towards (or nearby) the pelvis, we defined θ_{ref} to be the angle between the selected endpoint (see Table II) and the pelvis.

3) *Data normalization*: The cost function (Equation 8) is basically a weighted sum of the above-described metrics. To prevent one metric from having a larger influence on the total cost than another, normalization of the metrics was performed, using the z-score normalization method. MATLAB's built-in `zscore`-function was used for this, where the z-score is computed by

$$z = \frac{(x - \nu)}{\sigma} \quad (13)$$

where ν and σ are the mean and standard deviation of the dataset and x is the data point for which the z-score is being computed. After z-score normalization, the data set typically

has a mean of zero and a standard deviation of one. Therefore, the costs we will eventually compute could be negative, which might seem odd, but a negative cost should just be interpreted as a low cost.

We would like to emphasize again that the above-mentioned torque trajectories, fatigue indices, and manipulability measures are all computed in 2D, in the sagittal plane, since 3D analysis falls outside of the scope of this research.

Thus, to summarize how this all comes together in the cost function, an example is provided: the torque metric for the right hip T_{hip_r} was computed for all 45 recorded gaits, then normalized to $T_{hip_r}^*$ using Equation 13. Finally, T_{total}^* was computed by a weighted sum over all the joints. This T_{total}^* can be seen as the cost term associated with the joint torque, presented as $\sum_{i=1}^n (w_{t,i} \cdot T_i)$ in the cost function. Note that S_{total}^* and O_{total}^* are computed by averaging over the gait phases, whereas T_{total}^* and U_{total}^* are computed by averaging over the joints.

4) *Brute-force optimization*: There are numerous strategies available in literature that have been applied in gait optimization, each having its pros and cons. Evolutionary approaches have been explored [58]–[61], which are inspired by biological evolution. Also, function optimization methods have been applied [62], [63], that aim to find the input to a given function that results in the minimum or maximum output from the function. However, many approaches share the drawback of being plagued by local optima. To ensure finding a global minimum, we apply brute-force optimization. In contrast with other optimization methods, that have a strategy to determine which point in the solution space will be evaluated next, brute-force optimization evaluates all points in the solution space. Normally, the big drawback of this method is the lengthy computation time. However, as mentioned in Section II-A, the volume of the search space for the optimization problem at hand is gravely reduced as it is only filled with our own, by motion capture acquired, gaits. In practice, this means that total cost H from Equation 8 is computed for each recorded gait and the gait with the lowest cost is selected as the optimal gait.

III. RESULTS

A set of seven gaits was chosen from the recorded motion data to display the effects of the gait parameters (stride length, step height, and walking speed) on the metrics (joint torque T , joint fatigue U , and manipulability ellipse shape S and orientation O). These gaits are: LowLowMid, MidLowMid, HighLowMid, MidMidMid, MidHighMid, MidLowLow, and MidLowHigh. These were selected since this set enables us to isolate the effect of altering one of the gait parameters, while keeping the other two gait parameters constant, like this:

- Stride length: LowLowMid, MidLowMid, HighLowMid
- Step height: MidLowMid, MidMidMid, MidHighMid
- Walking speed: MidLowLow, MidLowMid, MidLowHigh

Note that the natural gait (defined by a medium stride length, low step height, and medium walking speed, so MidLowMid) is present in each row in the above overview, so the observed results can always be compared to the natural gait.

As the manipulability is only dependent on the leg configurations the gaits MidLowMid, LowLowMid, HighLowMid, LowHighMid, and HighHighMid are analyzed for the manipulability, as these are the most extreme in terms of leg configurations. Since varying just the walking speed will not affect the manipulability, the selected gaits all have a medium walking speed. Furthermore, as the manipulability analysis on walking as performed in this research includes analyzing each gait event, it might be a bit too extensive to analyze all five above-mentioned gaits. Therefore, only the natural gait is thoroughly analyzed here, whereas the full analysis can be found in Appendix D.

A. Visualisation of recorded gaits

Figure 4 shows the joint angles for the hip, knee, and ankle of the dominant leg for one gait cycle, resulting from the IK process in OpenSim. In each column the natural gait is depicted (together with two other gaits), making it possible to compare each analyzed gait to the natural gait. Furthermore, in Figure 5, the leg configurations during relevant gait events are visualized.

A higher stride length seems to result in a larger range of motion (ROM) for the hip, knee and ankle during the swing phase (TO-IC2) and in a larger ROM for the ankle during the stance phase (IC-TO). Increasing the step height has the same effect on the hip and the knee joints but an opposite effect on the ankle during the swing phase. During the stance phase, no difference in ROM is noticed for all the joints. Altering the walking speed does not seem to have a clear effect on the joint angle trajectories.

B. Joint angle and joint torque verification

To get a sense of the reliability of the inverse kinematics (IK) and inverse dynamics (ID) processes, the percentage errors (PEs) of the joint angle and joint torque trajectories of the hips, knees, and ankles of five gaits (MidLowMid, LowLowHigh, BentLowHighMid, LeaningForwardMidHighMid, and HighHighLow) were computed, as explained in Section II-C. Table III gives the average PEs for each gait (so averaged over the six joints). It can be seen that all the PEs, for the joint angles as well as for the joint torques, stay below 4%.

TABLE III
PERCENTAGE ERRORS (PEs) FOR THE JOINT ANGLES AND JOINT TORQUES.

Gait	Average PE (%)	Average PE (%)
	Joint angles	Joint torques
MidLowMid	1.54	1.28
LowLowHigh	1.42	3.24
BentLowHighMid	3.77	2.24
LeaningForwardMidHighMid	1.35	2.17
HighHighLow	0.80	1.79

C. Effect of gait parameters on metrics

1) *Joint torque*: The joint torque trajectories, obtained from ID in OpenSim, are shown in Figure 6. First of all, it stands

out that in all plots of the knee and hip, a spike can be seen at initial contact of the dominant leg. For the ankle, this spike is present as well but very small. A medium stride length seems to induce the largest hip torque during OIC, followed by a high and then a low stride length. The same holds for the ankle torque. During terminal swing, a medium stride length induces the most negative torque in the hip and knee, whereas a high and low stride length have a less negative torque. The high stride length even induces a small positive torque for the hip. For the ankle, the medium and high stride length gaits have quite similar trajectories, while the low stride length stands out with a much smaller torque around OIC.

When the step height decreases, a higher hip torque is observed around OIC. The same holds for the knee, but this effect is less prominent. During terminal swing, a high step height results in a positive torque in the hip, a low one in a negative torque, and a medium one in a torque close to zero. For the knee, a lower step height induces a more negative torque during terminal swing. Moreover, in initial swing, the knee and hip torque trajectories seem to give a larger negative torque than the medium and low step heights. Around OTO a low and medium step height result in positive knee torques, whereas the high step height results in a negative one. The torque at the ankle joint does not seem to be affected much by changes in the step height. Finally, the peaks at initial contact of the dominant leg seem to be larger for smaller step heights for the knee and hip joints.

Increasing the walking speed results in larger hip torques for the hip and knee during loading response and mid-stance. For the hip, around OIC a high and medium speed result in higher torques compared to the lower speed. The same effect is seen for the hip and knee during terminal swing. During initial swing, the medium and high speeds result in positive torques, whereas the low speed results in a negative torque. Finally, The ankle trajectory seems quite unaffected by the speed, except during mid-stance, where the low speed has the lowest torque, the medium speed has the highest torque, and the high speed remains in between the other two trajectories.

In Table IV T_{total}^* (i.e. the cost associated with the torque) is presented for the seven displayed gaits. Note that, due to the normalization process, negative cost values can occur (as explained in Section II-F3). These can simply be interpreted as low costs. We see a clear trend that increasing the stride length (LowLowMid \rightarrow MidLowMid \rightarrow HighLowMid) results in a higher torque cost. When increasing the step height (MidLowMid \rightarrow MidMidMid \rightarrow MidHighMid), we see a similar trend. For an increasing walking speed (MidLowLow \rightarrow MidLowMid \rightarrow MidLowHigh) no such trend is seen.

2) *Joint fatigue*: Figure 7 displays the fatigue index u computed using Equation 4. It can be seen that when the torque trajectories from Figure 6 exceed their thresholds τ_{thr} (depicted as horizontal dashed lines in Figure 6), the fatigue index u increases. Moreover, when these torque trajectories stay under their thresholds, u seems to stay nearly constant. Table IV shows the U_{total}^* (i.e. the cost associated with the fatigue) for each of the seven analyzed gaits. For an increasing stride length (LowLowMid \rightarrow MidLowMid \rightarrow HighLowMid) an increase in U_{total}^* is seen. Especially LowLowMid stands

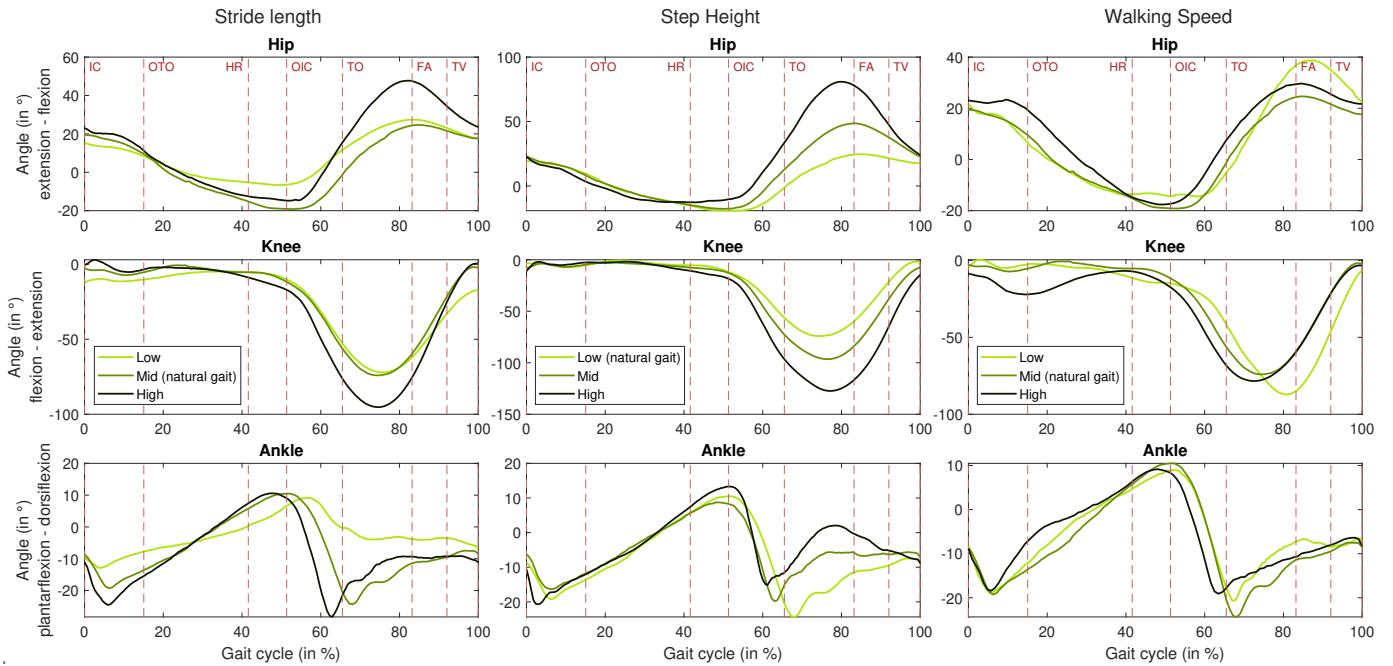


Fig. 4. The effect of the stride length (left column), step height (middle column), and walking speed (right column) on the joint angles during walking. To clarify: in the left column, LowLowMid, MidLowMid, and HighLowMid are depicted, in the middle column, MidLowMid, MidMidMid, and MidHighMid, and in the right column, MidLowLow, MidLowMid, and MidLowHigh. Relevant gait events are indicated by the red dashed lines. Note that these can slightly differ per gait, however only the gait events of the natural gait are shown to keep the figure organized.

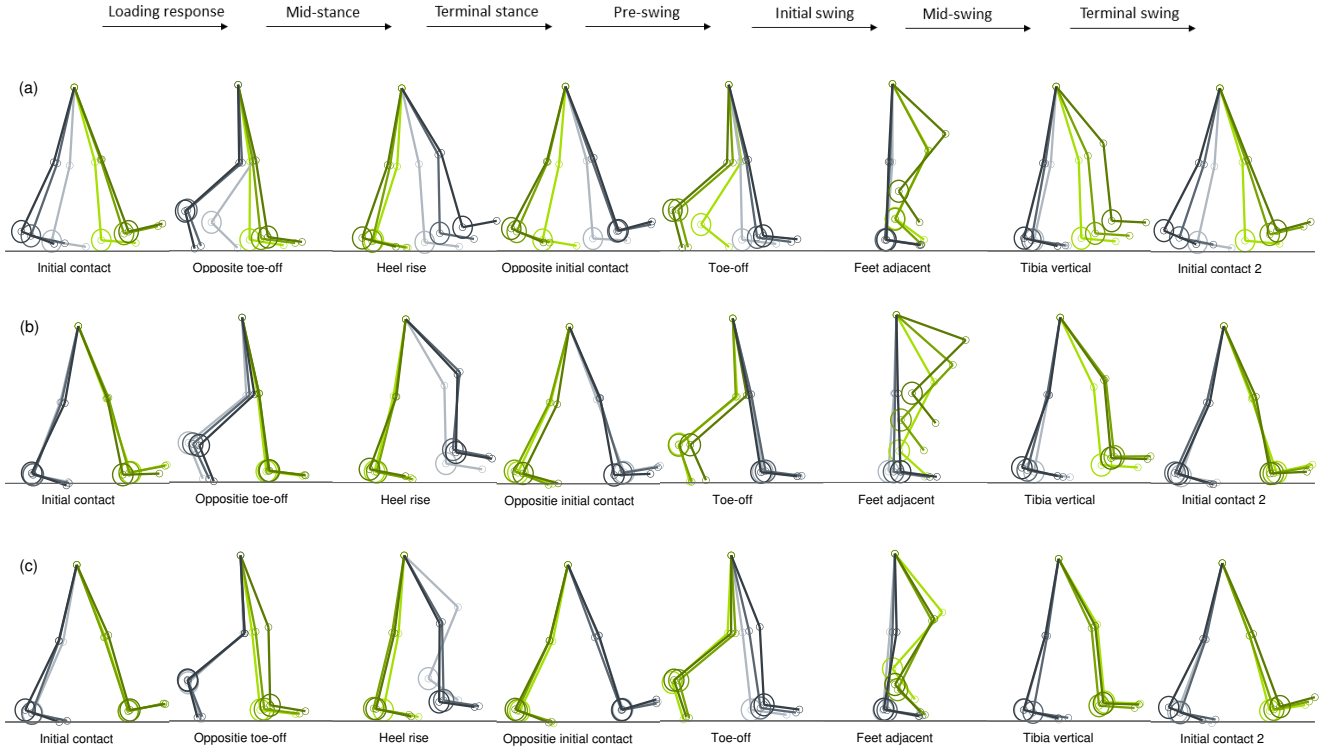


Fig. 5. Visualization of the leg configurations at the relevant gait events during one gait cycle, starting and ending with initial contact. The gaits visualizing the effect of different (a) stride lengths are LowLowMid (lightest color), MidLowMid (medium-dark color), and HighLowMid (darkest color), only differing in stride length, having similar walking speed and step height. Different (b) step heights are visualized by MidLowMid (lightest color), MidMidMid (medium-dark color), and MidHighMid (darkest color), only differing in step height, having similar walking speed and stride length. Different (c) walking speeds are visualized by MidLowLow (lightest color), MidLowMid (medium-dark color), and MidLowHigh (darkest color), only differing in walking speed, keeping the stride length and step height the same. The dominant leg is indicated by green shades and the supporting leg by gray shades.

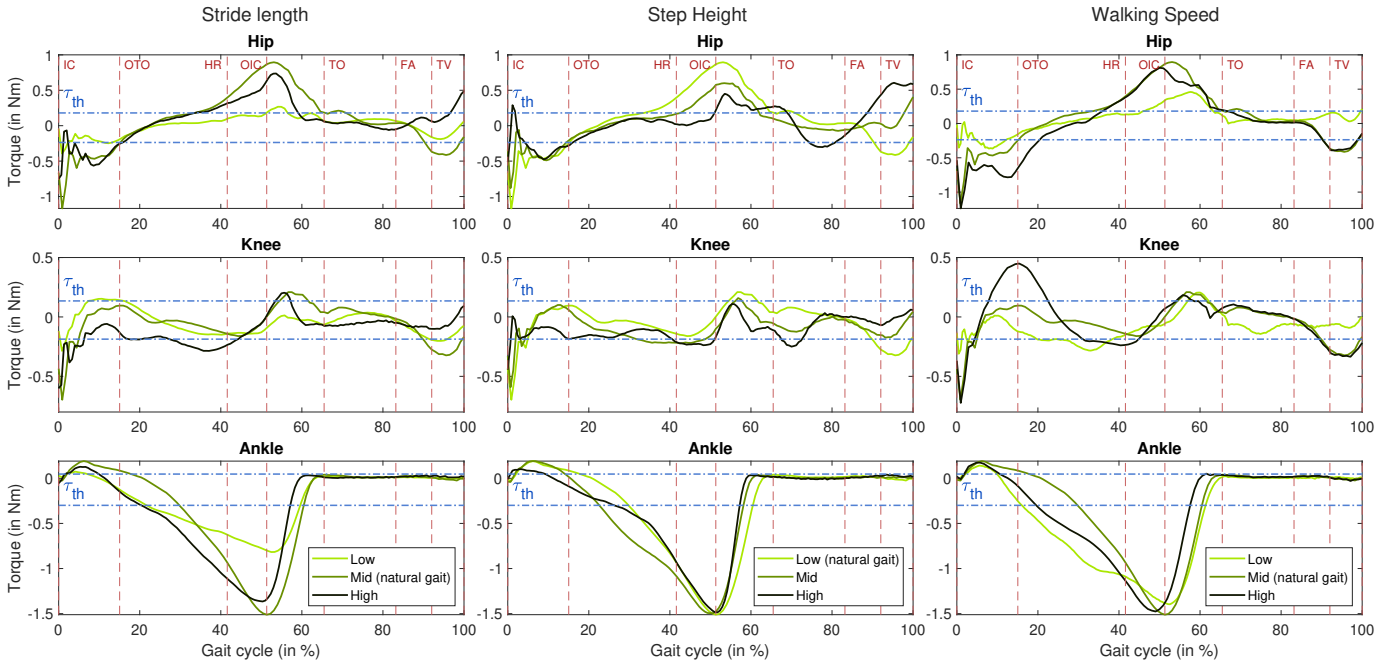


Fig. 6. The effect of the stride length (left column), step height (middle column), and walking speed (right column) on the joint torque trajectories. To clarify: in the left column, LowLowMid, MidLowMid, and HighLowMid are depicted, in the middle column, MidLowMid, MidMidMid, and MidHighMid, and in the right column, MidLowLow, MidLowMid, and MidLowHigh. Torque thresholds τ_{th} (see Table I), relevant for the joint fatigue, are indicated by blue dashed lines. Gait events are indicated by the red dashed lines. Note that these can slightly differ per gait, however only the gait events of the natural gait are shown to keep the figure organized.

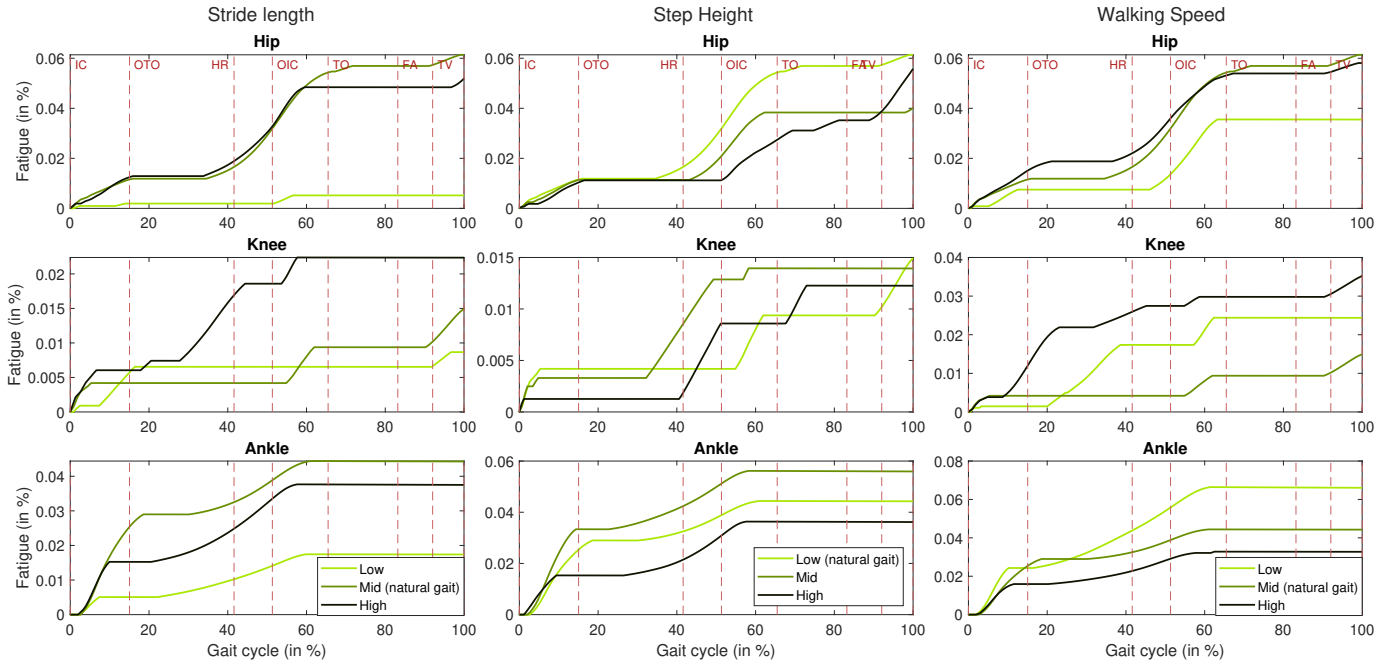


Fig. 7. Effect of stride length (left column), step height (middle column), and walking speed (right column) on the joint fatigue. The left column shows LowLowMid, MidLowMid, and HighLowMid, the middle column shows MidLowMid, MidMidMid, and MidHighMid, and the right column shows MidLowLow, MidLowMid, and MidLowHigh. Gait events of the natural gait are indicated by the red dashed lines.

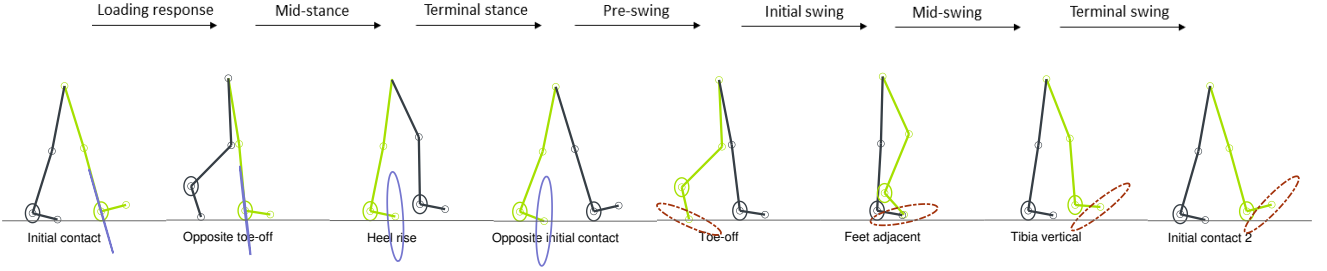


Fig. 8. The force ellipse (blue solid line) and velocity ellipse (red dashed line) for the relevant gait events of the natural gait MidLowMid are visualized. For the stance phase, i.e. IC until TO, the force ellipse is drawn, while for the swing phase, i.e. TO until IC2, the velocity ellipse is drawn. The dominant leg is indicated by green and the supporting leg by gray. Furthermore, the ellipse drawn for the gait events IC and OTO is centered on the heel, whereas the others are centered on the toe, as explained in Table II.

TABLE IV
TOTAL COSTS PER METRIC, TOGETHER WITH OVERALL TOTAL COST H , GIVEN FOR THE SEVEN GAITS TREATED IN THIS SECTION.

Gait	T^*_{total}	U^*_{total}	S^*_{total}	O^*_{total}	Total cost (H)
MidLowMid	-0.418	-0.459	0.18	-0.188	-0.885
MidLowLow	-0.215	-0.289	0.624	-0.34	-0.220
MidLowHigh	0.391	-0.280	0.0854	0.106	0.303
MidMidMid	-0.393	-0.508	-0.0587	-0.135	-1.09
MidHighMid	-0.268	-0.492	-0.28	-0.366	-1.41
LowLowMid	-1.16	-1.24	0.182	-0.499	-2.72
HighLowMid	-0.0759	-0.316	0.318	0.0263	-0.048

out with a fatigue cost much lower than the others. Changing the step height does not seem to have a clear effect on the fatigue cost. Increasing and decreasing the walking speed (MidLowMid \rightarrow MidLowHigh, MidLowMid \rightarrow MidLowLow) both seem to increase the fatigue cost.

3) *Manipulability*: In Figure 8, the force/velocity ellipses are visualized for each gait event during the gait cycle of the natural gait (MidLowMid). Only the analysis of this natural gait is shown to provide a general impression of what the proposed manipulability analysis on walking looks like. Appendix D contains similar figures for the gaits LowLowMid, HighLowMid, HighHighMid, and LowHighMid, might the reader be interested in seeing the effect of different walking motions on the force/velocity ellipses.

It can be seen in Figure 8 that the force ellipses, drawn for IC, OTO, heel rise (HR) and OIC, point very closely towards the pelvis, which is the reference point for the force ellipse orientation O during stance phase (explained in Section II-F). For the velocity ellipses, drawn for TO, feet adjacent (FA), tibia vertical (TV) and IC2, the reference direction for ellipse orientation O is parallel to the ground (explained in Section II-F). It can be seen that the velocity ellipse for FA points closely in this direction. For TO, TV and IC the velocity ellipses have a larger deviation from this reference direction.

The ellipse shape S is quite comparable for all the gait events, except for IC and OTO, where the ellipse is very stretched. In Table V the computed metrics S and O are given for the natural gait, quantifying what is shown in Figure 8. Note that the information in the figure and the table can not be compared directly with each other as the figure shows the gait events, whereas the table shows the average values of the metrics for the gait phases, which are the periods between the

gait events. Most notable in Table V is that, during loading response and mid-stance, very high values for S and very low values for O can be seen. Moreover, O seems to increase quite drastically throughout the gait cycle, especially during swing phase, whereas S stays quite constant during swing phase.

TABLE V
METRICS T AND U , GIVEN FOR EACH JOINT AND METRICS S AND O , GIVEN FOR EACH GAIT PHASE OF THE NATURAL GAIT (MIDLLOWMID).

Joint	T (Nm)	U (%)	Gait phase	S (-)	O ($^\circ$)
Hip right	0.320	0.0614	Loading response	59.4	0.528
Hip left	0.309	0.0589	Mid-stance	148	0.313
Knee right	0.113	0.0149	Terminal stance	4.38	2.76
Knee left	0.0957	0.0140	Pre-swing	5.28	1.37
Ankle right	0.332	0.0443	Initial swing	5.18	11.0
Ankle left	0.249	0.0374	Mid-swing	6.02	19.0
			Terminal swing	5.32	36.0

D. Multi-metric optimization

In Table V an overview is given of the metrics T , U , S and O computed for the natural gait. Table VI gives a similar overview, but with the normalized metric values (T^* , U^* , S^* and O^*) and a weighted sum for each metric is provided, representing the total cost of that metric for the natural gait. Then in Table IV, the total costs of each metric (T^*_{total} , U^*_{total} , S^*_{total} and O^*_{total}) are presented for the seven gaits treated in this section and the overall total cost H is provided for each gait. Note that all the weights used for computing the values presented in Table IV are set to one in this case (as explained in Section II-F1).

TABLE VI
NORMALIZED METRICS T^* , U^* , S^* AND O^* , GIVEN FOR THE NATURAL GAIT (MIDLLOWMID).

Joint	T^*	U^*	Gait phase	S^*	O^*
Hip right	0.0734	-0.221	Loading response	-0.172	-0.767
Hip left	0.0589	-0.268	Mid-stance	0.0903	-0.734
Knee right	-0.811	-0.821	Terminal stance	-0.0909	1.29
Knee left	-0.957	-0.795	Pre-swing	0.358	0.116
Ankle right	-0.132	-0.301	Initial swing	1.43	0.608
Ankle left	-0.742	-0.346	Mid-swing	1.85	-1.13
			Terminal swing	-1.39	-0.692
Weighted sum	-0.418	-0.459	Weighted sum	0.180	-0.188

From Table IV it can be seen that LowLowMid has the lowest cost, followed by MidHighMid. The highest cost is seen for MidLowHigh, followed by HighLowMid. LowLowmid seems to score especially well on torque and fatigue, which are the largest costs seen in the table. In Appendix E a table similar to Table IV is shown, but for all 45 recorded gaits.

IV. DISCUSSION

A new framework for multi-metric gait optimization is proposed, applicable for different contexts and goals, accounting for joint torque, fatigue, and manipulability. To ensure that the framework would always select a physiological and stable gait, a database of motion capture recorded gaits was formed, serving as a solution space for the optimization process.

By combining several metrics in the optimization, this framework facilitates preventing the joints to be overloaded, ensuring that motion and force can be produced/sustained well during different phases of the gait, and taking into account the long-term performance of the gait, simultaneously.

The database of recorded motions should contain substantial variation in terms of the gait parameters (stride length, step height, and walking speed), to form a good representation of the search space for optimization. Figures 4 and 5 verify that variations in terms of stride length and step height are represented well in the data set. Variation in walking speed is not visible in these figures as they are presented with respect to phase rather than time. However, Table VII in Appendix B does verify the presence of variation in walking speed and also confirms the presence of stride length and step height variations.

Moreover, the results showed that different gaits result in different costs for the individual metrics, as well as for the overall cost H (see Table IV). Since the costs, presented in this table, are computed with all the optimization weights set to one, the result functions as a baseline for tuning the framework. It can be used to analyze the gait patterns, in particular getting some insight into which aspect of the gait is responsible for a good or bad overall performance. For example, LowLowMid performs best in the baseline case, especially due to very low torque and fatigue costs, indicating that the joints are not loaded heavily and that this gait can be sustained for a long time. As LowLowMid is the gait with the least extreme leg configurations of the seven presented gaits (low stride length and low step height), this makes sense. When we look at MidHighMid, a good performance in terms of manipulability is noticed, which indicates that the leg configurations are quite optimal for sustaining external loads during the stance phase and for advancing the limb during the swing phase. A more thorough discussion on the effect of the gait parameters on the metrics, can be found in Appendix F.

While the optimization weights are intentionally set to one in this study to function as a baseline for analysis, eventually, the purpose of these weights is to provide a tool for the user to translate their requirements for a desired gait pattern into an optimization goal for the framework. However, further research into details of how to tune the weights for specific user requirements is needed.

Our proposed framework provides a new method to analyze and optimize the gait for multiple metrics at the same time, as opposed to many previous studies that only optimize for one metric [32], [33], [35], [38], [39]. Moreover, while fatigue has been included in gait optimization indirectly through minimizing energy efficiency [39], [40], we accounted for fatigue directly by applying a fatigue model. While fatigue modeling has been studied for applications in the field of ergonomics and manufacturing (with focus on the legs or the whole body) [41], [44], our framework applies it in gait optimization, focusing on the legs.

In this study, we limited our gait analysis to the sagittal plane, which is a common approach in literature [64], [65]. However, such an approach gives us no insight into the performance of the gait in the other planes, possibly excluding valuable information. For example, the hip joints play a critical role in maintaining balance of the trunk in the frontal plane [66], which can not be analyzed by sagittal plane analysis. Furthermore, this 2D assumption results in a less accurate motion description, as the number of degrees of freedom is reduced, thus a less complete reflection of the motion is presented. Therefore, future research could improve the framework by incorporating 3D analysis.

In the computation of the torque thresholds and λ values for the fatigue model, bilateral symmetry of the legs was assumed, equalling both legs to the weakest one. Although bilateral symmetry might be a decent assumption in healthy individuals, there is typically a much larger difference in leg functionality for individuals with a leg injury. In such a case, we want to minimize the risk of worsening the injury, therefore the conservative assumption of basing the fatigue characteristics of both legs on the capability of the weakest leg still seems like the best option.

Furthermore, for determining the torque threshold values, a fatigue index of 20% was assumed after half an hour of regular walking. Since no research has been performed that suggests a reasonable estimate of fatigue index after a specified time of walking, an additional study is recommended to better calibrate the fatigue model.

In the current method, joint torque metric T is computed by the mean of the absolute joint torque trajectory. Therefore, a gait pattern with a low torque cost could still contain some high peak torque values in the torque trajectories. To improve this, the addition of another set of torque thresholds is advised, specifying a maximum allowed torque and filtering out gaits when this value is exceeded at any moment.

Finally, like in many other studies, the issue of model accuracy is a bottleneck in the proposed framework. However, due to the modularity of the framework, it is possible for better models to be incorporated, allowing the framework to keep improving.

V. CONCLUSION

We successfully created a gait optimization framework, taking into account joint torque, fatigue, and manipulability. A baseline case was presented that can be used to analyze the performance of gait patterns, which enables gathering

insights into specific aspects of the gait. Future research into properly tuning the weights for specific user requirements is recommended to improve the framework's potential to select well-fitting gaits for users with specific needs.

REFERENCES

- [1] J. Amato, *On Foot: A History of Walking*. NYU Press, Nov. 2004, google-Books-ID: tAKaV3EwIJQC.
- [2] J. John M. Schuna and C. Tudor-Locke, "Step by step: accumulated knowledge and future directions of step-defined ambulatory activity," *Research in Exercise Epidemiology*, vol. 14, no. 2, pp. 107–116, 2012.
- [3] D. H. Sutherland, "The evolution of clinical gait analysis part I: kinesiological EMG," *Gait & Posture*, vol. 14, no. 1, pp. 61–70, Jul. 2001.
- [4] M. W. Whittle, "Clinical gait analysis: A review," *Human Movement Science*, vol. 15, no. 3, pp. 369–387, Jun. 1996.
- [5] K. K. Patterson, N. K. Nadkarni, S. E. Black, and W. E. McIlroy, "Gait symmetry and velocity differ in their relationship to age," *Gait & Posture*, vol. 35, no. 4, pp. 590–594, Apr. 2012.
- [6] J. R. Gage, "Gait analysis. An essential tool in the treatment of cerebral palsy," *Clinical orthopaedics and related research*, no. 288, pp. 126–134, Mar. 1993.
- [7] V. L. Chester, E. N. Biden, and M. Tingley, "Gait Analysis," *Biomedical Instrumentation & Technology*, vol. 39, no. 1, pp. 64–74, Jan. 2005.
- [8] P. Eichelberger, M. Ferraro, U. Minder, T. Denton, A. Blasimann, F. Krause, and H. Baur, "Analysis of accuracy in optical motion capture - A protocol for laboratory setup evaluation," *Journal of Biomechanics*, vol. 49, no. 10, pp. 2085–2088, Jul. 2016.
- [9] M. Field, D. Stirling, F. Naghdy, and Z. Pan, "Motion capture in robotics review," in *2009 IEEE International Conference on Control and Automation*, Dec. 2009, pp. 1697–1702, iSSN: 1948-3457.
- [10] M. Roberts, D. Mongeon, and F. Prince, "Biomechanical parameters for gait analysis: a systematic review of healthy human gait," *Physical Therapy and Rehabilitation*, vol. 4, p. 6, Jan. 2017.
- [11] G. S. Rash, "Electromyography: Fundamentals," in *International Encyclopedia of Ergonomics and Human Factors - 3 Volume Set*, 2nd ed. CRC Press, 2006.
- [12] V. Agostini, M. Ghislieri, S. Rosati, G. Balestra, and M. Knafitz, "Surface Electromyography Applied to Gait Analysis: How to Improve Its Impact in Clinics?" *Frontiers in Neurology*, vol. 11, 2020.
- [13] D. Shi, W. Zhang, W. Zhang, and X. Ding, "A Review on Lower Limb Rehabilitation Exoskeleton Robots," *Chinese Journal of Mechanical Engineering*, vol. 32, no. 1, p. 74, Aug. 2019.
- [14] M. Fahmi Bin Miskon and M. B. A. J. Yusof, "Review of trajectory generation of exoskeleton robots," in *2014 IEEE International Symposium on Robotics and Manufacturing Automation (ROMA)*, Dec. 2014, pp. 12–17.
- [15] X. Zhang, Z. Yue, and J. Wang, "Robotics in Lower-Limb Rehabilitation after Stroke," *Behavioural Neurology*, vol. 2017, p. e3731802, Jun. 2017, publisher: Hindawi.
- [16] A. Rodríguez-Fernández, J. Lobo-Prat, and J. M. Font-Llagunes, "Systematic review on wearable lower-limb exoskeletons for gait training in neuromuscular impairments," *Journal of NeuroEngineering and Rehabilitation*, vol. 18, no. 1, p. 22, Feb. 2021.
- [17] W.-Z. Li, G.-Z. Cao, and A.-B. Zhu, "Review on Control Strategies for Lower Limb Rehabilitation Exoskeletons," *IEEE Access*, vol. 9, pp. 123 040–123 060, 2021, conference Name: IEEE Access.
- [18] A. Esquenazi and M. Talaty, "Robotics for Lower Limb Rehabilitation," *Physical Medicine and Rehabilitation Clinics*, vol. 30, no. 2, pp. 385–397, May 2019, publisher: Elsevier.
- [19] D. R. Louie and J. J. Eng, "Powered robotic exoskeletons in post-stroke rehabilitation of gait: a scoping review," *Journal of NeuroEngineering and Rehabilitation*, vol. 13, no. 1, p. 53, Jun. 2016.
- [20] H.-J. Kim, D.-H. Lim, W.-S. Kim, and C.-S. Han, "Development of a Passive Modular Knee Mechanism for a Lower Limb Exoskeleton Robot and Its Effectiveness in the Workplace," *International Journal of Precision Engineering and Manufacturing*, vol. 21, no. 2, pp. 227–236, Feb. 2020.
- [21] C. J. Walsh, K. Endo, and H. Herr, "A quasi-passive leg exoskeleton for load-carrying augmentation," *International Journal of Humanoid Robotics*, vol. 04, no. 03, pp. 487–506, Sep. 2007, publisher: World Scientific Publishing Co.
- [22] J. E. Pratt, B. T. Krupp, C. J. Morse, and S. H. Collins, "The RoboKnee: an exoskeleton for enhancing strength and endurance during walking," in *IEEE International Conference on Robotics and Automation, 2004. Proceedings. ICRA '04. 2004*, vol. 3, Apr. 2004, pp. 2430–2435 Vol.3, iSSN: 1050-4729.
- [23] A. Gams, T. Petrič, T. Debevec, and J. Babič, "Effects of Robotic Knee Exoskeleton on Human Energy Expenditure," *IEEE Transactions on Biomedical Engineering*, vol. 60, no. 6, pp. 1636–1644, Jun. 2013, conference Name: IEEE Transactions on Biomedical Engineering.
- [24] S. H. Collins, M. B. Wiggin, and G. S. Sawicki, "Reducing the energy cost of human walking using an unpowered exoskeleton," *Nature*, vol. 522, no. 7555, pp. 212–215, Jun. 2015, number: 7555 Publisher: Nature Publishing Group.
- [25] A. Esquenazi, M. Talaty, A. Packel, and M. Saulino, "The ReWalk Powered Exoskeleton to Restore Ambulatory Function to Individuals with Thoracic-Level Motor-Complete Spinal Cord Injury," *American Journal of Physical Medicine & Rehabilitation*, vol. 91, no. 11, pp. 911–921, Nov. 2012.
- [26] E. Strickland, "Good-bye, wheelchair," *IEEE Spectrum*, vol. 49, no. 1, pp. 30–32, Jan. 2012, conference Name: IEEE Spectrum.
- [27] B. Chen, C.-H. Zhong, X. Zhao, H. Ma, X. Guan, X. Li, F.-Y. Liang, J. C. Y. Cheng, L. Qin, S.-W. Law, and W.-H. Liao, "A wearable exoskeleton suit for motion assistance to paralysed patients," *Journal of Orthopaedic Translation*, vol. 11, pp. 7–18, Oct. 2017.
- [28] D. Popović, M. Radulović, L. Schwirtlich, and N. Jauković, "Automatic vs hand-controlled walking of paraplegics," *Medical Engineering & Physics*, vol. 25, no. 1, pp. 63–73, Jan. 2003.
- [29] S. Jezernik, G. Colombo, T. Keller, H. Frueh, and M. Morari, "Robotic Orthosis Lokomat: A Rehabilitation and Research Tool," *Neuromodulation: Technology at the Neural Interface*, vol. 6, no. 2, pp. 108–115, 2003.
- [30] K. Miura, M. Morisawa, F. Kanehiro, S. Kajita, K. Kaneko, and K. Yokoi, "Human-like walking with toe supporting for humanoids," in *2011 IEEE/RSJ International Conference on Intelligent Robots and Systems*, Sep. 2011, pp. 4428–4435, iSSN: 2153-0866.
- [31] P. Fitzpatrick, K. Harada, C. C. Kemp, Y. Matsumoto, K. Yokoi, and E. Yoshida, "Humanoids," in *Springer Handbook of Robotics*, ser. Springer Handbooks, B. Siciliano and O. Khatib, Eds. Cham: Springer International Publishing, 2016, pp. 1789–1818.
- [32] J. Zhang, P. Fiers, K. A. Witte, R. W. Jackson, K. L. Poggensee, C. G. Atkeson, and S. H. Collins, "Human-in-the-loop optimization of exoskeleton assistance during walking," *Science*, vol. 356, no. 6344, pp. 1280–1284, Jun. 2017, publisher: American Association for the Advancement of Science.
- [33] P. H. Channon, S. H. Hopkins, and D. T. Pham, "A Variational Approach To The Optimization of Gait For a Bipedal Robot," *Proceedings of the Institution of Mechanical Engineers, Part C: Journal of Mechanical Engineering Science*, vol. 210, no. 2, pp. 177–186, Mar. 1996, publisher: IMEChE.
- [34] T. Yoshikawa, "Manipulability of Robotic Mechanisms," *The International Journal of Robotics Research*, vol. 4, no. 2, pp. 3–9, Jun. 1985, publisher: SAGE Publications Ltd STM.
- [35] B. Miripour Fard and S. M. Bruijn, "On the manipulability of swing foot and stability of human locomotion," *Multibody System Dynamics*, vol. 46, no. 2, pp. 109–125, Jun. 2019.
- [36] B. Miripour Fard, "A manipulability analysis of human walking," *Journal of Biomechanics*, vol. 83, pp. 157–164, Jan. 2019.
- [37] B. M. Fard and M. Mosadeghzad, "Manipulability Based Hierarchical Control of Perturbed Walking," *International Journal of Control, Automation and Systems*, vol. 17, no. 9, pp. 2343–2353, Sep. 2019.
- [38] W. Kim, S. Lee, M. Kang, J. Han, and C. Han, "Energy-efficient gait pattern generation of the powered robotic exoskeleton using DME," in *2010 IEEE/RSJ International Conference on Intelligent Robots and Systems*, Oct. 2010, pp. 2475–2480, iSSN: 2153-0866.
- [39] Z. Liu, L. Wang, C. L. P. Chen, X. Zeng, Y. Zhang, and Y. Wang, "Energy-Efficiency-Based Gait Control System Architecture and Algorithm for Biped Robots," *IEEE Transactions on Systems, Man, and Cybernetics, Part C (Applications and Reviews)*, vol. 42, no. 6, pp. 926–933, Nov. 2012.
- [40] I. Lim, O. Kwon, and J. H. Park, "Gait optimization of biped robots based on human motion analysis," *Robotics and Autonomous Systems*, vol. 62, no. 2, pp. 229–240, Feb. 2014.
- [41] L. Peternel, N. Tsagarakis, D. Caldwell, and A. Ajoudani, "Robot adaptation to human physical fatigue in human-robot co-manipulation," *Autonomous Robots*, vol. 42, no. 5, pp. 1011–1021, Jun. 2018.
- [42] P. Maurice, V. Padois, Y. Measson, and P. Bidaud, "Experimental assessment of the quality of ergonomic indicators for dynamic systems

- computed using a digital human model," *International Journal of Human Factors Modelling and Simulation*, vol. 5, no. 3, p. 190, 2016.
- [43] E. Lamon, A. De Franco, L. Peternel, and A. Ajoudani, "A Capability-Aware Role Allocation Approach to Industrial Assembly Tasks," *IEEE Robotics and Automation Letters*, vol. 4, no. 4, pp. 3378–3385, Oct. 2019, conference Name: IEEE Robotics and Automation Letters.
- [44] L. Peternel, D. T. Schön, and C. Fang, "Binary and Hybrid Work-Condition Maps for Interactive Exploration of Ergonomic Human Arm Postures," *Frontiers in Neurobotics*, vol. 14, 2021, publisher: Frontiers.
- [45] M. Peasgood, J. McPhee, and E. Kubica, "Stabilization and Energy Optimization of a Dynamic Walking Gait Simulation." American Society of Mechanical Engineers Digital Collection, Jun. 2008, pp. 339–349.
- [46] M. Tucker, E. Novoseller, C. Kann, Y. Sui, Y. Yue, J. W. Burdick, and A. D. Ames, "Preference-Based Learning for Exoskeleton Gait Optimization," in *2020 IEEE International Conference on Robotics and Automation (ICRA)*, May 2020, pp. 2351–2357.
- [47] K. A. Ingraham, C. D. Remy, and E. J. Rouse, "The role of user preference in the customized control of robotic exoskeletons," *Science Robotics*, vol. 7, no. 64, p. eabj3487, Mar. 2022.
- [48] F. L. Haufe, S. Maggioni, and A. Melendez-Calderon, "Reference Trajectory Adaptation to Improve Human-Robot Interaction: A Database-Driven Approach," in *2018 40th Annual International Conference of the IEEE Engineering in Medicine and Biology Society (EMBC)*, Jul. 2018, pp. 1727–1730.
- [49] A. Seth *et al.*, "OpenSim: Simulating musculoskeletal dynamics and neuromuscular control to study human and animal movement," *PLoS Computational Biology*, vol. 14, no. 7, p. e1006223, Jul. 2018, publisher: Public Library of Science.
- [50] J. J. Eng and D. A. Winter, "Kinetic analysis of the lower limbs during walking: What information can be gained from a three-dimensional model?" *Journal of Biomechanics*, vol. 28, no. 6, pp. 753–758, Jun. 1995.
- [51] M. A. Giese and T. Poggio, "Morphable Models for the Analysis and Synthesis of Complex Motion Patterns," *International Journal of Computer Vision*, vol. 38, no. 1, pp. 59–73, Jun. 2000.
- [52] L. Ma, D. Chablat, F. Bennis, and W. Zhang, "A new simple dynamic muscle fatigue model and its validation," *International Journal of Industrial Ergonomics*, vol. 39, no. 1, pp. 211–220, Jan. 2009.
- [53] J. Ding, A. S. Wexler, and S. A. Binder-Macleod, "A predictive model of fatigue in human skeletal muscles," *Journal of Applied Physiology*, vol. 89, no. 4, pp. 1322–1332, Oct. 2000, publisher: American Physiological Society.
- [54] Y. Giat, J. Mizrahi, and M. Levy, "A musculotendon model of the fatigue profiles of paralyzed quadriceps muscle under FES," *IEEE Transactions on Biomedical Engineering*, vol. 40, no. 7, pp. 664–674, Jul. 1993, conference Name: IEEE Transactions on Biomedical Engineering.
- [55] J. Z. Liu, R. W. Brown, and G. H. Yue, "A Dynamical Model of Muscle Activation, Fatigue, and Recovery," *Biophysical Journal*, vol. 82, no. 5, pp. 2344–2359, May 2002.
- [56] N. Vahrenkamp, T. Asfour, G. Metta, G. Sandini, and R. Dillmann, "Manipulability analysis," in *2012 12th IEEE-RAS International Conference on Humanoid Robots (Humanoids 2012)*, Nov. 2012, pp. 568–573.
- [57] D. Levine, J. Richards, and M. W. Whittle, *Whittle's Gait Analysis*. Elsevier Health Sciences, Jul. 2012.
- [58] S. Chernova and M. Veloso, "An evolutionary approach to gait learning for four-legged robots," in *2004 IEEE/RSJ International Conference on Intelligent Robots and Systems (IROS) (IEEE Cat. No.04CH37566)*, vol. 3, Sep. 2004, pp. 2562–2567 vol.3.
- [59] G. S. Hornby, M. Fujita, S. Takamura, T. Yamamoto, and O. Hanagata, "Autonomous evolution of gaits with the sony quadruped robot," in *Proceedings of the 1st Annual Conference on Genetic and Evolutionary Computation-Volume 2*. Citeseer, 1999, pp. 1297–1304.
- [60] J. Kim, D. X. Ba, H. Yeom, and J. Bae, "Gait Optimization of a Quadruped Robot Using Evolutionary Computation," *Journal of Bionic Engineering*, vol. 18, no. 2, pp. 306–318, Mar. 2021.
- [61] D. Gong, J. Yan, and G. Zuo, "A review of gait optimization based on evolutionary computation," *Applied Computational Intelligence and Soft Computing*, 2010, publisher: Hindawi.
- [62] M. S. Kim and W. Uther, "Automatic Gait Optimisation for Quadruped Robots," in *In Australasian Conference on Robotics and Automation*, 2003.
- [63] Y. Xiang, J. S. Arora, and K. Abdel-Malek, "Optimization-based prediction of asymmetric human gait," *Journal of Biomechanics*, vol. 44, no. 4, pp. 683–693, Feb. 2011.
- [64] C. P. C. Chen *et al.*, "Sagittal Plane Loading Response During Gait in Different Age Groups and in People with Knee Osteoarthritis," *American Journal of Physical Medicine & Rehabilitation*, vol. 82, no. 4, pp. 307–312, Apr. 2003.
- [65] J. Park, M. K. Seeley, D. Francom, C. S. Reese, and J. T. Hopkins, "Functional vs. Traditional Analysis in Biomechanical Gait Data: An Alternative Statistical Approach," *Journal of Human Kinetics*, vol. 60, no. 1, pp. 39–49, Dec. 2017.
- [66] C. D. MacKinnon and D. A. Winter, "Control of whole body balance in the frontal plane during human walking," *Journal of Biomechanics*, vol. 26, no. 6, pp. 633–644, Jun. 1993.
- [67] J. S. V. Sint, "Color atlas of skeletal landmark definitions," *Guidelines for reproducible manual and virtual palpations, Edinburgh: Churchill Livingstone*, pp. 29–175, 2007.

APPENDIX

A. Motion Capture Experiment: Optical marker locations

The experiment was performed using a full-body marker set of 44 markers, as seen in Figure 9, based on [67]. Eventually, 32 markers were used for the IK process in OpenSim, since the markers that were added to the arms were eventually not used in the remainder of the project.

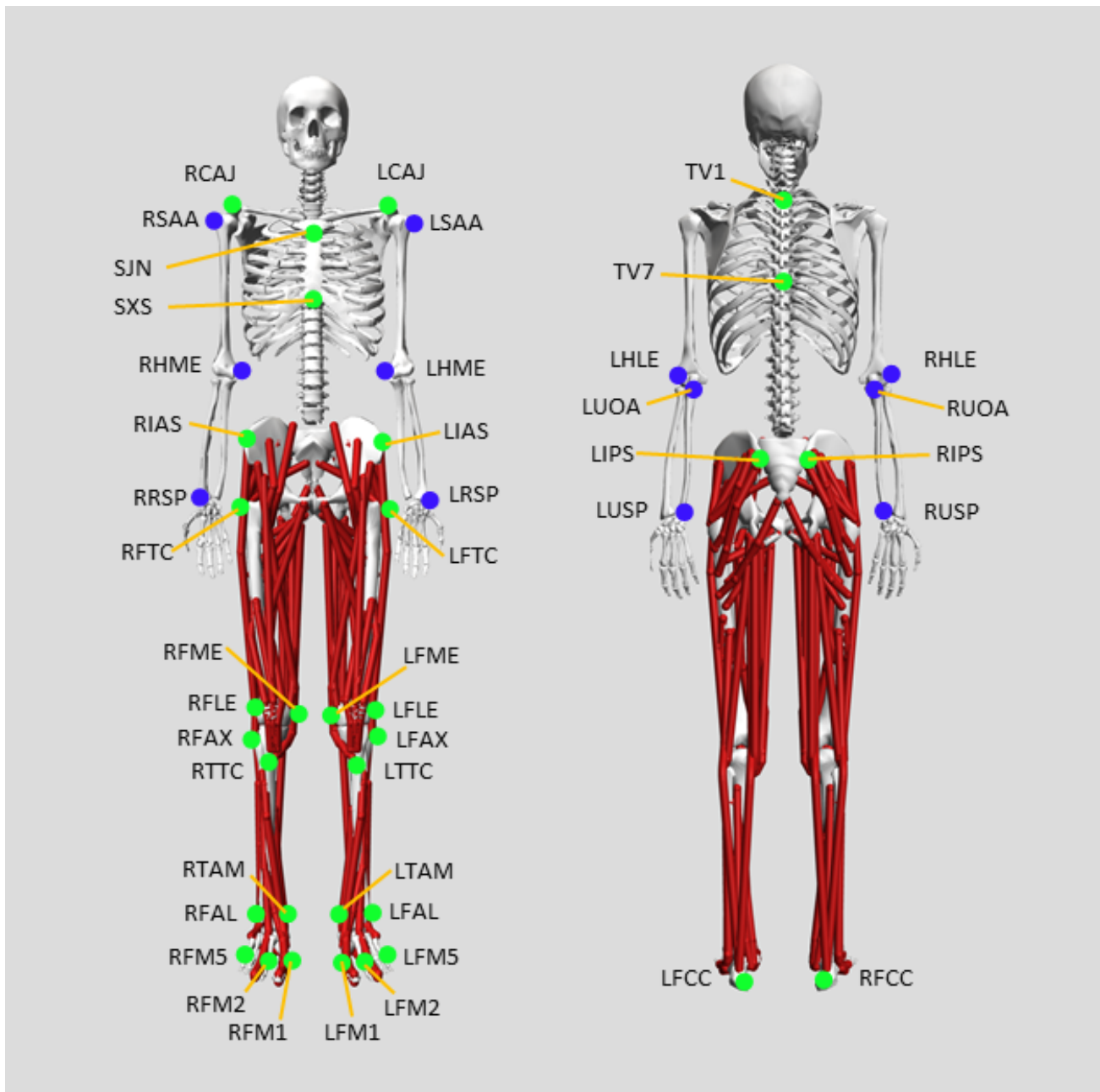


Fig. 9. Schematic image of the locations of the 44 reflective optical markers during the recordings. The 12 markers placed on the arms (indicated in blue) were eventually not used in the remainder of this research, in contrast to the 32 markers on the rest of the body (indicated in green). The generic gait 2392 OpenSim model was used to create this image.

B. Gait parameters recorded gaits

Here an overview is given of the data set, containing all 45 recorded gaits, together with the computed values for stride length, step height, walking speed, and cadence. The gaits MidLowMid until HighHighHigh form the basic data set, whereas the gaits BentMidLowMid until LeaningForwardHighHighMid form the additional data set, as explained in Section II-B2.

TABLE VII
GAIT PARAMETERS, COMPUTED FOR ALL 45 GAITS RECORDED DURING THE MOTION CAPTURE EXPERIMENT.

Gait	Stride length (m)	Step height (m)	Walking speed (m/s)	Cadence (s^{-1})
MidLowMid	0,585	0,366	1,09	106
MidLowLow	0,575	0,399	0,554	55,8
MidLowHigh	0,661	0,388	1,42	115
MidMidMid	0,59	0,442	0,877	82,2
MidMidLow	0,573	0,465	0,57	59,1
MidMidHigh	0,543	0,526	0,893	104
MidHighMid	0,547	0,663	0,679	70,6
MidHighLow	0,63	0,617	0,489	47,8
MidHighHigh	0,58	0,703	0,862	93,7
LowLowMid	0,298	0,325	0,54	98,4
LowLowLow	0,305	0,441	0,305	57,7
LowLowHigh	0,328	0,379	0,638	112
LowMidMid	0,365	0,541	0,411	78,4
LowMidLow	0,334	0,66	0,336	55
LowMidHigh	0,292	0,597	0,56	106
LowHighMid	0,311	0,683	0,335	63,5
LowHighLow	0,298	0,663	0,246	46,5
LowHighHigh	0,297	0,689	0,469	91,6
HighLowMid	0,711	0,442	1,01	79,5
HighLowLow	0,707	0,355	0,721	55,3
HighLowHigh	0,759	0,372	1,44	100
HighMidMid	0,718	0,493	0,937	72,7
HighMidLow	0,694	0,444	0,679	55,3
HighMidHigh	0,762	0,531	1,14	94,5
HighHighMid	0,733	0,58	0,872	67,4
HighHighLow	0,737	0,617	0,794	60,3
HighHighHigh	0,74	0,658	1,17	86,3
BentMidLowMid	0,55	0,345	0,893	86,3
BentMidHighMid	0,587	0,523	0,82	80
BentLowLowMid	0,289	0,313	0,419	78,9
BentLowHighMid	0,289	0,522	0,395	75,9
BentHighLowMid	0,73	0,457	1,09	77,9
BentHighHighMid	0,743	0,534	1,01	73,2
LeaningBackMidLowMid	0,583	0,355	0,794	76,9
LeaningBackMidMidMid	0,594	0,466	0,743	75,5
LeaningBackMidHighMid	0,561	0,601	0,746	74,1
LeaningBackLowLowMid	0,356	0,343	0,377	72,7
LeaningBackLowMidMid	0,378	0,48	0,347	69,8
LeaningBackLowHighMid	0,321	0,663	0,365	66,7
LeaningForwardMidLowMid	0,632	0,399	0,98	85,1
LeaningForwardMidHighMid	0,585	0,6	0,773	75
LeaningForwardLowLowMid	0,274	0,308	0,414	83,9
LeaningForwardLowHighMid	0,282	0,544	0,419	82,2
LeaningForwardHighLowMid	0,643	0,361	1,02	86,3
LeaningForwardHighHighMid	0,676	0,586	0,993	74,5

C. Joint fatigue parameter estimation

In total, 12 calibration experiments were performed, determining fatigue parameter λ for each joint (hip, knee, and ankle of both legs), in flexion and extension direction. In Figure C the experimental setup of each of the calibration experiments is shown. In each measurement, the subject was instructed to push his/her limb into a force sensor (model: FTS-Delta SI-330-30, manufacturer: Schunk GmbH & Co. KG, Germany). Only in the measurement where calibration of the ankle in plantar flexion was performed, a different procedure was followed, which will be explained later in this section. The relation between joint torque τ and measured force F_{meas} is given by

$$\tau = F_{meas} \cdot d, \quad (14)$$

where d is the distance between the center of the concerned joint and the point of contact with the force sensor. Right before each measurement, d was measured.

The subject was instructed to produce maximum torque and maintain this torque level for as long as possible. Real-time visual feedback of the measured force was provided to the subject on a computer monitor. By keeping the measured force constant, the subject was able to maintain a constant torque level. The time T_{ref} was measured until the subject could not endure this torque level anymore. Note that this procedure is subject-dependant since the subject was instructed to stop when maintaining the torque level would become uncomfortable. Reference torque τ_{ref} could be computed by

$$\tau_{ref} = F_{ref} \cdot d, \quad (15)$$

where F_{ref} is the average measured force during time T_{ref} . Finally, fatigue parameter λ could be computed using Equation 5, given in Section II-D. Table VIII gives an overview of all estimated λ values and reference torques τ_{ref} . This table also presents the torque thresholds τ_{th} that are included in the fatigue model. Section II-D explains how those were computed.

To achieve the most realistic estimation of λ , the contribution of the concerned joint to the measured force F_{meas} should be completely isolated. Fully isolating the contribution of one joint during a task is very difficult, however, we attempted to isolate the joints as much as possible with the body configurations shown in Figure C.

Ankle plantar flexion calibration: Since we expected the plantar flexion moment, produced by the ankle, to induce a force larger than the force sensor could handle, this measurement was performed without a force sensor. Instead, the subject was instructed to carry a known mass, a barbell, while standing on a wooden step. In this case, distance d was the distance between the center of the ankle joint and the contact point of the foot with the wooden step. The maximum barbell mass that could be carried by the subject was 90 kg. A slightly larger mass might have been possible as well, however for safety reasons we did not exceed 90 kg. Reference force F_{ref} was determined by

$$F_{ref} = \frac{m_s + m_b}{2 \cdot g}, \quad (16)$$

where m_s and m_b are the mass of the subject and the barbell, respectively, and g is the gravitational constant. As the subject is carrying the mass with both legs in this experiment, the reference torque is produced by both ankles. Since we want to compute λ for each ankle separately, division by 2 can be seen in Equation 16. Similar as in the other experiments, time T_{ref} was measured until the subject could not endure the load anymore and Equations 15 and 5 were used to determine the λ values.

TABLE VIII
REFERENCE TORQUES PRODUCED BY THE SUBJECT DURING THE CALIBRATION EXPERIMENTS.

		Hip flexion	Knee flexion	Ankle dorsiflexion	Hip extension	Knee extension	Ankle plantar flexion
τ_{ref} (Nm)	Right leg	67.81	53.77	17.68	109.48	76.76	111.25
	Left leg	66.82	50.05	17.42	88.02	69.38	111.25
λ (Nms)	Right leg	444	282	92.6	88.2	57.8	2.15e+3
	Left leg	552	282	75.8	75.3	55.0	2.15e+3
τ_{th} (Nm)	Right leg	0.180	0.142	0.047	-0.291	-0.204	-0.295
	Left leg	0.177	0.133	0.046	-0.234	-0.184	-0.295

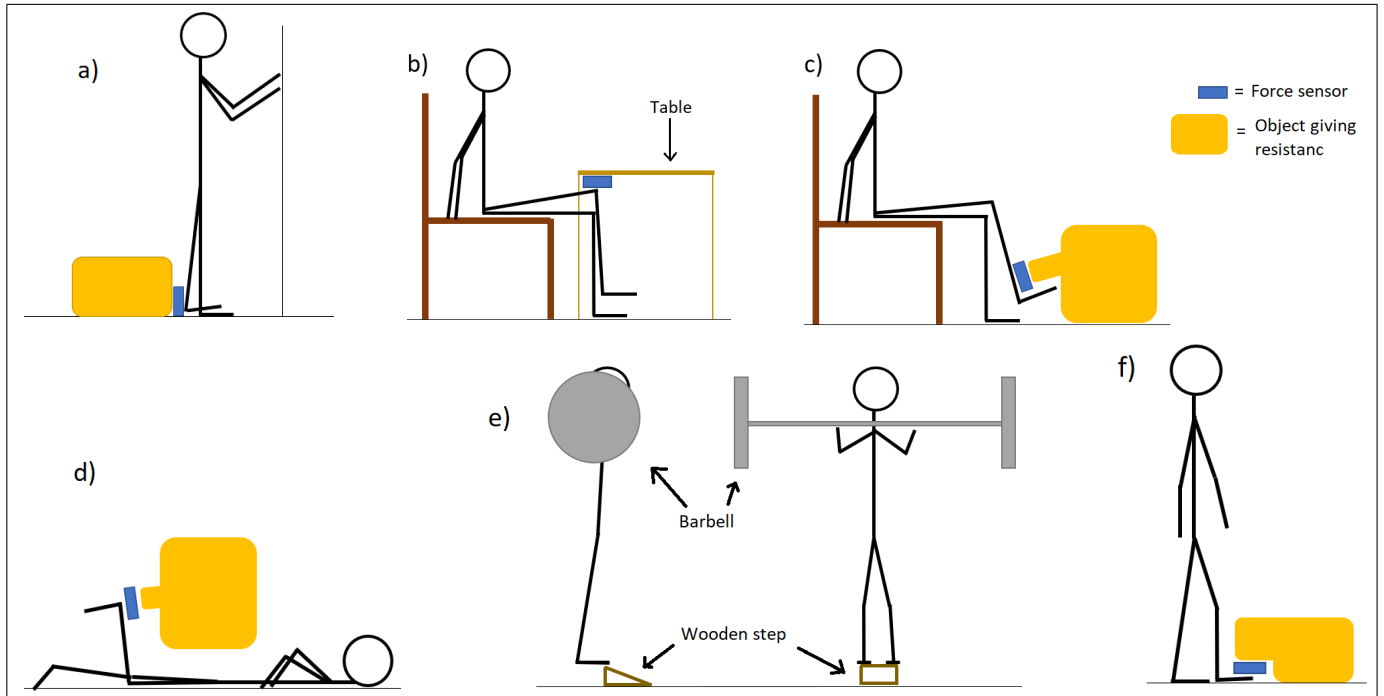


Fig. 10. Schematic visualization of the experimental setup during the calibration experiments, to determine joint-specific fatigue parameter λ for (a) hip extension, (b) hip flexion, (c) knee extension, (d) knee flexion, (e) ankle plantar flexion, and (f) ankle dorsiflexion.

D. Manipulability analysis results

In Figure 11 the force/velocity ellipses are visualised for each gait event during the gait cycle, for five gaits. The natural gait (MidLowMid) is depicted, as well as gaits with a low/high stride length and a low/high step height. This selection was made as the variations in leg configuration between those gaits are the largest, when considering the basic data set. Considering that the manipulability is only configuration dependent, no variations in walking speed are shown in Figure 11, since varying the walking speed is not expected to have a significant effect on the leg configurations during walking.

First of all it stands out that the majority of the ellipses are quite stretched, indicating a high ellipse shape S , especially during IC and OTO. Moreover, the ellipse shapes of IC, OTO, HR and OIC seem very similar for each of the five gaits. During swing phase, the velocity ellipse shape shows more variability, especially in FA, where it is less stretched for HighLowMid (c), LowHighMid (d), and HighHighMid (e).

During stance phase, a very similar ellipse orientation O is seen for the five presented gaits. The most significant difference can be spotted in OIC, where the orientation for LowLowMid (b) and LowHighMid (d) seems shifted counterclockwise slightly. During swing phase, more variation in ellipse orientation is seen. For all the gait events during swing phase, the ellipses drawn for LowLowMid (b) and LowHighMid (d) seem to be oriented more towards the reference angle (parallel to the ground), especially for TO and IC2.

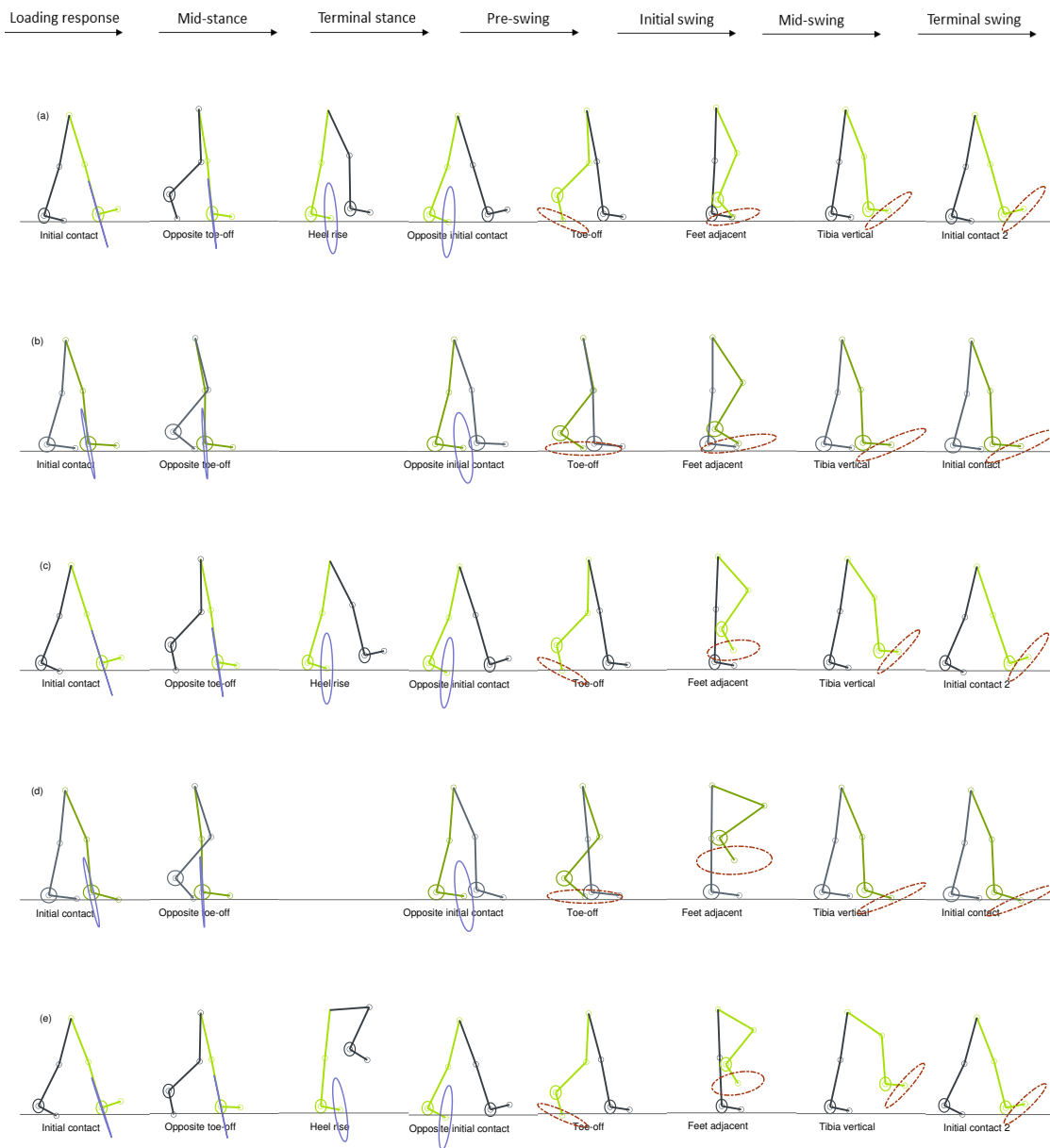


Fig. 11. The force ellipse (blue solid line) and velocity ellipse (red dashed line) for the relevant gait events of several gaits are visualised. The gaits depicted are: The natural gait MidLowMid (a), LowLowMid (b), HighLowMid (c), LowHighMid (d) and HighHighMid (e). For the stance phase, i.e. initial contact until toe-off, the force ellipse is drawn, while for the swing phase, i.e. toe-off until initial contact, the velocity ellipse is drawn. The dominant leg is indicated by green and the supporting leg by gray. Furthermore, the ellipse drawn for the gait events initial contact (IC) and opposite toe-off (OTO) are centered on the heel, whereas the others are centered on the toe, as explained in Table II. Heel rise (HR) is not displayed for LowLowMid and LowHighMid as for these gaits this gait event occurs after opposite initial contact (OIC) and displaying it would be confusing for the reader.

E. Elaborate cost table

Below the cost table is shown with the total costs for all metrics (T_{total}^* , U_{total}^* , S_{total}^* and O_{total}^*), with the overall total cost H and with a ranking from 1 to 45 indicating the most optimal gait with 1 and the least optimal gait with 45. Note that the values presented in this table are computed with a weighting of one assigned to all the weights, as explained in Section II-F1.

TABLE IX
TOTAL COSTS PER METRIC, TOGETHER WITH OVERALL TOTAL COST H , FOR ALL 45 RECORDED GAITS.

Gait	T_{total}^*	U_{total}^*	S_{total}^*	O_{total}^*	Total cost (H)	Ranking
MidLowMid	-0.418	-0.459	0.18	-0.188	-0.885	17
MidLowLow	-0.215	-0.289	0.624	-0.34	-0.22	18
MidLowHigh	0.391	-0.28	0.0854	0.106	0.303	26
MidMidMid	-0.393	-0.508	-0.0587	-0.135	-1.09	15
MidMidLow	-0.313	-0.384	1.22	-0.196	0.326	27
MidMidHigh	-0.605	-0.58	-0.108	-0.451	-1.74	9
MidHighMid	-0.268	-0.492	-0.28	-0.366	-1.41	11
MidHighLow	-0.174	0.186	0.158	0.205	0.375	29
MidHighHigh	-0.354	-0.268	-0.361	-0.362	-1.35	12
LowLowMid	-1.16	-1.24	0.182	-0.499	-2.72	4
LowLowLow	-0.88	-1.08	0.0261	-0.163	-2.1	6
LowLowHigh	-1.4	-1.27	0.189	-0.595	-3.07	1
LowMidMid	-1.01	-1.18	-0.151	-0.594	-2.93	3
LowMidLow	-0.625	-0.79	-0.199	-0.452	-2.07	7
LowMidHigh	-0.988	-1	-0.258	-0.752	-3	2
LowHighMid	-0.439	-0.758	-0.0966	-0.715	-2.01	8
LowHighLow	-0.443	-0.248	-0.149	-0.452	-1.29	13
LowHighHigh	-0.864	-0.914	0.0653	-0.404	-2.12	5
HighLowMid	-0.0759	-0.316	0.318	0.0263	-0.0481	20
HighLowLow	0.264	0.257	0.603	0.255	1.38	32
HighLowHigh	0.342	-0.0535	0.338	0.56	1.19	31
HighMidMid	-0.152	-0.107	0.124	0.0546	-0.0798	19
HighMidLow	-0.255	-0.00186	0.493	-0.0813	0.155	23
HighMidHigh	-0.0717	-0.106	0.529	-0.0705	0.281	25
HighHighMid	0.198	0.261	0.588	0.482	1.53	35
HighHighLow	0.262	0.625	0.246	0.418	1.55	36
HighHighHigh	0.354	0.305	-0.0354	0.274	0.898	30
BentMidLowMid	1.28	0.619	-0.247	0.684	2.34	43
BentMidHighMid	1.32	1.23	-0.97	1.27	2.85	44
BentLowLowMid	0.738	0.544	-0.631	0.866	1.52	34
BentLowHighMid	1.09	0.814	-0.768	1.16	2.3	42
BentHighLowMid	1.13	1.03	-0.67	0.618	2.11	41
BentHighHighMid	1.62	1.45	-1.25	1.27	3.1	45
LeaningBackMidLowMid	0.512	1.68	0.197	-0.29	2.09	40
LeaningBackMidMidMid	0.186	1.6	-0.0934	-0.2	1.49	33
LeaningBackMidHighMid	0.455	1.46	0.163	-0.315	1.76	37
LeaningBackLowLowMid	-0.991	-0.427	0.229	-0.271	-1.46	10
LeaningBackLowMidMid	-0.739	-0.124	0.047	-0.268	-1.08	16
LeaningBackLowHighMid	-0.569	-0.126	-0.139	-0.328	-1.16	14
LeaningForwardMidLowMid	0.397	-0.229	0.306	-0.314	0.161	24
LeaningForwardMidHighMid	0.0967	0.0318	-0.0137	-0.105	0.0101	21
LeaningForwardLowLowMid	0.387	-0.226	0.213	-0.29	0.0842	22
LeaningForwardLowHighMid	0.471	-0.0486	-0.0163	-0.0463	0.36	28
LeaningForwardHighLowMid	0.96	0.529	-0.235	0.654	1.91	39
LeaningForwardHighHighMid	0.937	0.888	-0.393	0.335	1.77	38

F. Elaborate discussion: Effect of gait parameters on metrics

1) *Joint torque:* Something that stands out when looking at the effect of the stride length on the joint torque is that the medium stride length (thus the natural gait) results in the highest torque for the hip and ankle around OIC. Since the low stride length clearly induces the lowest torque in the joints around this moment, it would seem logical for the high stride length to produce the highest torque, which is not the case. However, looking at the torque costs T_{total}^* from Table IV we do see this expected trend of an increasing torque for an increased stride length.

Another interesting effect can be seen around OIC of the hip, as for increasing step height, a lower torque is observed. This feels counter-intuitive, since larger movements are expected to result in higher joint torques, rather than lower ones. Once again, when we look at Table IV to analyze the effect of the step height on the torque, we see the expected result, as for higher step heights, higher torque costs are observed.

Lastly, for a high walking speed we see a very high knee torque around OTO, also clearly visible in Table IV with a high cost. This time no clear trend is seen in the cost table as the lowest torque is observed for the medium walking speed instead of the low one. An explanation could be that walking in the natural gait is the most relaxed gait and thus the least GRFs would arise, but this is speculation.

In general we could say that it is more difficult to detect a clear pattern of the effects of the gait parameters on the joint torques compared to the joint angles when purely visually analyzing the trajectories. However, using the table with computed torque costs it is possible to find some more expected trends, indicating that the torque metric might be a useful number in analyzing the joint torque.

2) *Joint fatigue:* In Figure 6 the torque thresholds, associated with the fatigue model are also displayed. As specified in Section II-D, the joints should experience an increase in fatigue when the torques exceed the threshold and should decrease in fatigue when torques stay within the thresholds. In Figure 7 it is seen that the switching between the fatigue increasing and decreasing mode works flawlessly. However, when in recovery mode, instead of seeing a decrease in the fatigue level it more or less stays constant. This can be explained by looking at the recovery part of Equation 4. There we see that the recovery increment is dependent on the fatigue level itself and as we are dealing only with fatigue levels of 0.07% or lower, this increment will always be almost negligible.

The reason that we only encounter such low fatigue levels is through our assumption that we start the analyzed gait cycle with a completely rested body, while in reality this is not the case. To be able to incorporate the effect of the recovery part of the fatigue model on the analysis as well, it might be interesting to try out different initial fatigue levels. Furthermore, the recovery constant selected in this research was purely based on previous works and could therefore lack in reflecting reality.

An interesting effect can be seen in the fatigue levels of the ankle in Figure 7, as the fatigue increases quite rapidly during loading response, whereas it increases more slowly during mid-stance and terminal stance. This might seem odd as the ankle torque produced during push-off (around OIC) is much larger than the torque produced during loading response. The cause of this is fatigue parameter λ , determined during the calibration experiments, which is much larger in plantar flexion direction than in dorsiflexion. A higher λ value means that more effort is required by the joint for fatigue to occur. Therefore, it makes sense that ankle plantar flexion has a higher λ as the ankle joints are much stronger and therefore better resistant to fatigue in this direction.

When looking in Table IV it is seen that increasing the stride length or the step height results in an increased fatigue cost. As performing larger motions requires more energy this seems to make sense. For the walking speed, the natural gait results in the lowest cost, indicating that increasing or decreasing the speed is more tiring for the legs. To walk at a higher speed, higher accelerations are also required, which are generated in the joints, so this also feels correct. According to this reasoning, walking slowly should result in a lower fatigue cost. However, to walk slowly, the limbs should be lifted longer, which could be the cause of this higher fatigue cost. This all suggests that the natural gait involves a walking speed that has found the right balance between these things and is quite energy-efficient.

3) *Manipulability:* As for the manipulability, the ellipse orientation during stance phase points quite closely towards its reference angle, the pelvis. This can be seen in Figure 8 and is confirmed by the low O values observed in Table V. Furthermore, the ellipse shape is quite flat during the stance phase. These two things mean that the stance leg is configured such that it can carry the bodyweight very efficiently during walking. This is not only the case for the natural gait, as Figure 11 in Appendix D shows similar ellipse orientations during the stance phase for the other analyzed gaits, suggesting that, no matter the walking motion, the body ensures that its weight can be carried efficiently by the legs.

For the velocity ellipse orientation more deviation from the reference angle (i.e. the ground) can be seen, as in initial swing the ellipse is oriented slightly downward and during terminal swing, the ellipse is tilted upward. When thinking purely in terms of motion, this does not make sense, as in initial swing the foot is lifted, thus an upward-pointing ellipse would be expected, and for terminal swing vice versa. Following this reasoning, the decision we made to point the reference angle for the velocity ellipses parallel to the ground might be a bit coarse and we suggest possible future works to reconsider this.

